OFFICE OF NAVAL RESEARCH

Grant or Contract N0014-95-1-0302
R&T Code 3132124

Technical Report No. 9

Synthesis and Physical Properties of Highly Sulfonated Polyaniline

by

X.-L. Wei, C. Bobeczko and A.J. Epstein

Prepared for publication in

Journal of the American Chemical Society

The Ohio State University
Department of Physics
Columbus, OH

March 1, 1996

Reproduction in while in part is permitted for any purpose of the United States Government

This document has been approved for public release and sale; its distribution is unlimited.

This statement should also appear in item ten (10) of the Document Control Data DD Form 1473. Copies of the form available from cognizant or contract administrator.

19960314 055

J. Am. Chem. Soc. XX, xx (1996)

Synthesis and Physical Properties of Highly Sulfonated Polyaniline

X.-L. Wei.

Chemical Physics Program

The Ohio State University

Columbus, Ohio 43210-1106

Y. Z. Wang and S. M. Long

Department of Physics

The Ohio State University

Columbus, Ohio 43210-1106

C. Bobeczko

Department of Chemistry

The Ohio State University

Columbus, Ohio 43210

A. J. Epstein

Department of Physics, Department of Chemistry,

and Chemical Physics Program

The Ohio State University

Columbus, Ohio 43210-1106

December 6, 1995

Abstract

Sulfonated polyaniline (EB-SPAN) is a self-doped conducting polymer. It has a high water solubility and a novel pH-dependent DC conductivity that is of interest for fundamental science and also for applications in such areas as rechargeable battery and pH control technologies. We report here the extensive characterization and details of synthesis of a new form of sulfonated polyaniline (LEB-SPAN) which shows novel or significantly improved chemical and physical properties. LEB-SPAN has a much high sulfur to nitrogen ratio (S/N) of $\sim$ 0.75, 50 % larger than that previously reported for EB-SPAN, S/N $\sim$ 0.50. This change in composition leads to significant alteration of the properties including an order of magnitude increase in the room temperature DC conductivity to $\sim$ 1 S·cm^{-1}, nearly double the solubility in water, and a completely different pH-dependence of the oxidation potential ($E_{1/2}$). For LEB-SPAN the DC conductivity is unaffected by pH over the range $0 \leq$ pH ≤ 14, strikingly different from the behavior of both parent polyaniline and EB-SPAN which become insulating for pH ≥ 3 and pH ≥ 7.5, respectively. Temperature-dependent DC conductivity and EPR measurements for LEB-SPAN reveal a lower activation energy for the conductivity and a higher density of states at the Fermi energy as compared with EB-SPAN. The dramatic differences in the pH-dependence of the DC conductivity, cyclic voltammetry (CV), FTIR, and UV-Vis results for LEB-SPAN and EB-SPAN are shown to be a consequence of the much higher S/N ratio in LEB-SPAN.

We propose and describe a novel *quasi quasi-random oxidation model* for the electrochemical oxidation of polyaniline and its derivatives at the microscopic level. This model quantitatively describes many of the phenomena and physical properties found in the polyanilines including the origin of the defect states and the *in situ* EPR signal during CV potential scans. Also the statistical nature of this model suggests its general applicability to the oxidation processes of other conducting polymers. Computer simulations based on this model are presented and show good agreement with the *in situ* EPR/CV data reported earlier. In addition other models are proposed to interpret the reported experimental differences in the pH-dependence of $E_{1/2}$ among LEB-SPAN, EB-SPAN, and its parent polyaniline samples. Mechanisms for the new sulfonation route are proposed.

Introduction

Sulfonated polyaniline (SPAN, the chemical structure in *Scheme 1*) is of interest because of its unusual electroactive physical properties, improved processability, and potential industrial applications [1-11]. SPAN is the first reported self-doped water soluble conducting polyaniline derivative and a prime model for dopant and secondary dopant induced processability [12, 13] in addition to self-doping [14]. It has been shown that SPAN has better thermal stability than its parent polyaniline doped with HCl [4]. It has been found that SPAN has potential use in rechargeable batteries with a higher charge density [5, 6] as compared to that obtainable utilizing the parent polyaniline [15, 16]. It has been reported that SPAN was used in fabricating a multilayer heterostructure light emitting diode devices [7]. SPAN also has potential for application in the electrochemical control of electrolyte acidity and enzyme activity [8]. In addition, SPAN has been proposed for use in patterning by coating a SPAN containing resist on a wafer [10].

A key control factor for the electroactive phenomena, processing, and potential applications is the degree of sulfonation, that is, the sulphur to nitrogen (S/N) ratio. A number of different synthetic routes earlier have been developed to achieve significant S/N ratios. Emeraldine base (EB) and pernigraniline base (PNB) forms of polyaniline (chemical structures in *Scheme 1*) have been used as starting materials for the preparation of SPAN (defined here as EB-SPAN and PNB-SPAN, respectively). Also fuming sulphuric acid, chlorosulfonic acid, and sulfur trioxide/triethyl phosphate complex have been reported as sulfonation agents in the synthesis of SPAN [3]. However, all of these earlier methods resulted in a maximum S/N ratio of 0.5.

The origins of some of the electroactive phenomena related to SPAN and parent polyaniline until now have remained unresolved. For example, the earlier reported [2] strong pH dependence of SPAN's first oxidation potential, $E_{1/2,1}$, differs from the pH independent behavor of $E_{1/2,1}$ of the parent polyaniline [17-20]. Also, cyclic voltammetry (CV) experiments and correlated *in situ* electron paramagnetic resonance (EPR) studies have been performed [18, 19, 21-25], however the variation of the *in situ* EPR intensity with the potential of the CV scan remains unexplained.

We report the detailed synthesis and characterization of very highly sulfonated polyaniline, using the most reduced form of polyaniline, leucoemeraldine base (LEB), as the starting material

(the final product is therefore termed LEB-SPAN). The LEB-SPAN has a higher S/N ratio, an order of magnitude greater DC conductivity, a different pH dependent oxidation potential, and other novel properties as compared with the parent polyaniline, EB-SPAN, and PNB-SPAN. A comparison of the results of FTIR, UV-Vis, pH dependence of CV and DC conductivity, temperature dependence of EPR and DC conductivity, and elemental chemical analysis of LEB-SPAN with earlier results for parent polyaniline, EB-SPAN, and PNB-SPAN is given, showing important ramifications of the higher S/N ratio for LEB-SPAN. A novel *quasi-random oxidation model* and mechanisms are proposed to account for electroactive phenomena of the polyanilines. The simulation result for the *in situ* EPR and CV spectra are presented and the different pH-dependent $E_{1/2}$ of LEB-SPAN, EB-SPAN, and parent polyaniline (PANI) are quantitatively interpreted based on the quasi-random oxidation model.

Experimental

The synthetic route for LEB-SPAN is described as follows [26]: Approximately 0.5 g of EB, prepared *via* the standard method [27], was mixed in a glass mortar with 2.5 ml of phenyl hydrazine. This mixture was pressed with a glass pestle for 5 minutes and stirred for one hour to facilitate the reduction of EB to LEB. It was then diluted with 75 ml ethyl ether, stirred for 15 minutes, filtered, washed with three 50 ml portions of ethyl ether, and suction dried. The dried LEB was then sulfonated in 10 ml of fuming sulfuric acid (pre-cooled to $\sim$ 5 C) for one hour. The reaction mixture was subsequently introduced into 0.75 liters of 75:25 ice-water mixture to precipitate the LEB-SPAN product. The product was then washed with three 250 ml portions of cold water. The LEB-SPAN powder was dried using a common procedure [27] at room temperature in a vacuum oven. The dried product was weighed and the yield was calculated to be $\sim$ 70%. The elemental chemical analyses (MHW Lab, Arizona) of LEB-SPAN found typical S/N ratios of $\sim$ 3/4.

The samples used for the pH-dependent conductivity measurements were prepared by dissolving LEB-SPAN powder in buffers of pH = 1 through 12 (50 mg/20 ml each) made in The Ohio State University Reagent Laboratory on October 10, 1994. LEB-SPAN samples for study at pH = 0 were prepared by dissolving in 1 M HCl, while samples for 12 $<$ pH $\leq$ 14 were

prepared by dissolving in NH_4OH or NaOH of appropriate pH. The resulting solutions were stirred for one day and then their pH was measured. Subsequently, these solutions were used to cast films on glass plates. The dried films were peeled off the glass substrates, further dried in a vacuum oven at 40° C for two days, and then pressed into pellets.

The temperature dependent DC conductivity measurements were performed using pressed pellets of SPAN powder utilizing a four probe technique [28]. The electron paramagnetic resonance measurements were carried out on powder samples using a Bruker ESP300 spectrometer. The UV-Vis spectra for the base form of LEB-SPAN were taken in 0.1 M aqueous NH_4OH solvent with a Perkin Elmer λ-19 spectrometer. The FTIR spectra of LEB-SPAN powder in pressed KBr pellets were acquired with a Mattson CYGNUS 100 spectrometer. The cyclic voltammograms were obtained on LEB-SPAN coated electrodes with a Hokto Corporation potentiostat/galvanostat (Model HA-301) and function generator (Model HB-111). These electrodes were prepared by coating Pt electrodes with solution of LEB-SPAN in 0.1 M NH_4OH solvent [2]. All of the studies of LEB-SPAN presented here were performed on samples from the same synthetic batch. Small variations in the physical properties were observed among different batches reflecting small differences in their S/N ratios.

Results and Discussion

The Mechanism and Rationale for the LEB Route

The chemical structures of the various oxidation states of parent PANI base and sulfonated polyaniline are shown in *Scheme 1*, where x and y denote the degree of polymerization and sulfonation (equivalent to S/N ratio), respectively. Based on the characterization of SPAN, a plausible sulfonation mechanism is proposed. For simplicity, we described here only the sulfonation mechanism for the unprotonated LEB repeat unit *Scheme 2*, (I) to (VI); the sulfonation mechanism for the protonated LEB repeat unit is proposed to be similar. In (I) two molecules of sulfuric acid interact to yield a solvated proton, an anion of sulfuric acid, and a molecule of sulfur trioxide. In (II) the oxidation of aniline unit by SO_3 is catalyzed by protons to yield an intermediate, (**a**). In (III) this intermediate rearranges to its more stable counterpart, sulfonated leucoemeraldine base, (**b**). In (IV) one repeat unit (**b**) is oxidized by the strong oxidant, fuming

sulfuric acid, to its quinoid counterpart, (**c**). Subsequently in (V) this quinoid unit is protonated either by the sulfonic acid group attached to the polymer backbone or by protons from solution to yield a bipolaron, (**d**). The bipolaron in (VI) could relax forming two semi-quinoid form polarons (**e**) which are free to separate further (for simplicity, only one of the polarons is shown in (e)). We have deliberately used different notations for the C_6 rings in (**d**) and in (**e**) to emphasize their different electronic structures. In (**d**) the originally six equivalent carbon-carbon bonds of the unperturbed benzene ring dimerize pairing the π-electrons, resulting in a doubly charged spinless bipolaron structure. However, in (**e**) the two charges and associated spins are shown centered on separate nitrogen atoms resulting in a net spin and hence an EPR signal.

The sulfonation of the phenyl rings is an electrophilic substitution reaction and therefore the larger electron density on the phenyl rings in the LEB route results in higher reaction rate, S/N ratio, and yield. In the EB and PNB routes when PANI is dissolved in fuming sulfuric acid the nitrogen atoms at quinoid sites are protonated. This causes the positive charges to delocalize into the quinoid ring units due to conjugation of the nitrogen p_z-orbital with the C_6 ring's π-orbitals. Therefore the positive charge can resonate between the protonated quinoid ring and nitrogen. The protonated imine repeat units are thus deactivated for the subsequent electrophilic aromatic substitution reaction, i.e. the sulfonation reaction. This may be the cause for the EB and PNB routes yielding typical S/N ratios of no more than 0.5. When the amine repeat units are protonated in sulfuric acid, the newly formed H-N bonds are of the sp^3 type localizing positive charge on the nitrogen sites due to reduced conjugation. Thus the resonance of positive charges into the benzene rings is minimal. The electron density within LEB's benzene rings in fuming sulfuric acid is higher so that electrophilic substitution on the ring occurs more easily than within EB and PNB. In addition, the Coulomb attraction of the positive charges on the the protonated imine nitrogen sites will result in a higher positive charge density on the adjacent carbon atoms in EB and PNB due to shorter bond lengths associated with the sp^2 orbital. Therefore the protonated imine unit is subject to greater hydrolysis than the amine unit and shorter polymer chain length will result for EB-SPAN and PNB-SPAN. It is not difficult to rationalize the higher S/N ratio and conductivity of typical LEB-SPAN over EB-SPAN and PNB-SPAN. Yue *et al* observed that the sulfonation level in EB-SPAN was higher than that of PNB-SPAN [3]. This supports our assumptions that the greater the electron

deficiency on the ring units the lower the S/N ratio of the sulfonated product thus resulting in a lower conductivity.

The oxidation of amine units and the sulfonation of phenyl rings can be thought of as competing reactions during the sulfonation of LEB. The higher S/N ratio of LEB-SPAN eliminates the possibility that substantial oxidation occurs before the sulfonation. If extensive oxidation occurred first the S/N ratio would be the same as for EB-SPAN. This experimental implication has been incorporated into *Scheme 2.* The rationale for protonation preceding oxidation is that protonation of amine atoms in the concentrated sulfuric acid has the effect of protecting the amine atoms from oxidation [29]. However, after the aniline repeat units are sulfonated the equilibrium shifts to favor deprotonation because: (1) Oxygen atoms or anions of the sulfonic acid group in the vicinity of the protonated amine atoms compete with amine nitrogen for protons. (2) The electron withdrawing nature of sulfonic acid makes the amine a weaker base. Therefore the oxidation of the amine atoms is more likely to occur after the sulfonation of the adjacent phenyl ring. Consequently, the oxidation state of LEB-SPAN can be either lower or higher than emeraldine salt depending on the sulfonation level, reaction time, and other reaction parameters.

Vibrational Spectra

The FTIR spectra of both LEB-SPAN and EB-SPAN are shown in Fig. 1. The number of peaks and their positions are essentially the same in both spectra while some of their relative intensities vary appreciably. The peaks at 1070 and 1040 cm^{-1} are assigned to aryl-S linkages, aromatic ring vibration having some C-S stretching characteristic. These peaks overlap a broad intense absorption extending from $\sim$ 850 cm^{-1} to $\sim$ 1200 cm^{-1}. It is evident that this broad absorption is a common feature of emeraldine salt and not a signature of the aryl-S linkages in SPAN, see Fig. 2. After subtracting the broad absorption, assumed to vary smoothly, from the LEB-SPAN spectrum, the ratio of the integrated intensity of the 1070 plus 1040 cm^{-1} peaks to that of the 1,500 plus 1,600 cm^{-1} peaks (stretches within the C_6 rings) is considerably larger than that found in EB-SPAN. In addition, the C-S stretching vibrational mode [3, 30] at 610 cm^{-1} in LEB-SPAN is more intense than in EB-SPAN. Thus we conclude that LEB-SPAN made *via* the current route has higher S/N ratio than that for EB-SPAN consistent with the elemental chemical analyses.

Electronic Spectra

The U v - Vis absorption bands of a dilute solution (0.3 mg/ml) of LEB-SPAN in aqueous 0.1 M NH_4OH are blue shifted relative to those of EB-SPAN in a similar solution (see Fig. 3). The benzenoid $\pi - \pi^*$ transition at 320 nm in EB-SPAN shifts to 312 nm in LEB-SPAN [31, 32]. Similarly the "exciton" transition in EB-SPAN at 541 nm shifts to 566 nm in LEB-SPAN [33]. The sulfonic acid groups substituted on the benzene rings cause an increase in the band gap due to their strong electron withdrawing nature. Also the higher sulfonation in LEB-SPAN results in larger steric strain increasing the torsional angle between adjacent rings [2, 31, 32]. This decreases the intrachain interaction leading to a further increase of the band gap. Thus, the UV-Vis data provides supporting evidence that sulfonation levels are higher in LEB-SPAN than in EB-SPAN. Another potential explanation for the blue-shift is that the spectrum effected by the oxidation that occurs during sulfonation. However, since the reactant, LEB, is more reduced than EB and a much smaller ratio of fuming sulfuric acid to phenyl ring units is used interference by increased oxidation is unlikely in the current route. In fact, approximately the same benzenoid ($\sim$ 1500 cm^{-1}) to quinoid ($\sim$ 1600 cm^{-1}) band intensity ratio was observed in the FTIR spectra of self-doped EB-SPAN and LEB-SPAN (Fig. 1).

Temperature-dependence of DC Conductivity

The room temperature DC conductivity of freshly prepared well ground LEB-SPAN (in pressed pellet form) was measured to be as high as $\sim$ 1 S/cm. The temperature dependence of the DC conductivity for LEB-SPAN is fit by the quasi-one-dimensional variable range hopping (quasi-1D-VRH) model [34]:

$$\sigma_{dc}(T) = \sigma_0 \exp[-(T_0/T)^{1/2}], \tag{1}$$

where $T_0 = 8\alpha/(z N(\epsilon_F) k_B)$, α^{-1} is the localization length, $N(\epsilon_F)$ is the density of states at the Fermi level, k_B is the Boltzmann constant, and z is the number of nearest neighbor chains. From Fig. 4 we obtain σ_0 = 780 S/cm, and $T_0 = 2.5 \times 10^4$ K. $\sigma(T)$ of EB-SPAN also fits [2] the quasi-1D-VRH model, however $T_0 \sim 3.9 \times 10^4$ K is larger than that of LEB-SPAN. This is consistent with the larger room-temperature conductivity for LEB-SPAN. Comparison of the experimental data to the 3D-VRH model [35], $T^{1/2}\sigma_{dc}(T) = A \exp[-B/T^{1/4}]$, and to the Arrhenius expression, $\sigma_{dc}(T) = C \exp[-D/T]$, did not yield good fits (A, B, C, and D are constants).

Temperature Dependence of Electron Paramagnetic Resonance

The EPR of LEB-SPAN has been measured. A single approximately Lorentzian line is observed over the experimental temperature range (3 K to 300 K). The full width at half maximum height linewidth of the absorption spectrum, ΔH_{FWHH}, decrease smoothly with increasing temperature from 4.9 G at 3 K to 1.0 G at 300 K (see Fig. 5). This trend is consistent with the observed increase in conductivity with increasing temperature assuming the EPR linewidth is narrowed by motional effects. That is, as the conductivity increases it is expected that there will be a corresponding increase in the motion of the unpaired electrons or spins resulting in more effective narrowing of the EPR line. Also in the limit of strong motional narrowing the EPR line shape approaches a Lorentzian consistent with our experimentally observed line shape. At room temperature the g-value calibrated against a 1,1′-diphenyl-2-picrylhydrazyl (DHHP) standard was found to be $\sim$ 2.0026. This g-value, typical of π radicals in conjugated carbon systems, is consistent with the unpaired spin delocalized primarily on phenyl rings [36, 37]. As the temperature decreases towards $\sim$ 70 K the g-value increases to $\sim$ 2.0030, a typical value for hetero-atom systems [38, 39], indicating that spins tend to become more localized at the nitrogen sites (see Fig. 6). This is consistent with the conductivity data and indicates greater localization at the lower temperatures.

The magnetic susceptibility as a function of temperature, χ(T), was obtained from the integrated intensity of the LEB-SPAN EPR signal calibrated against a DPPH standard. Plotting the susceptibility as $(\chi(T) \cdot T)$ *vs.* T (Fig. 7) the Curie and Pauli components were separated, assuming

$$\chi = \chi_{Pauli} + \chi_{Curie}, \tag{2}$$

where χ_{Pauli} is independent of temperature and χ_{Curie} is proportional T^{-1}. The Curie spin concentration was found to be 0.022 spins/two-rings. Based on the Pauli spin concentration the density of states at the Fermi level was calculated to be $N(\epsilon_F) \sim 1.0$ states/(eV two-rings) for each sign of the spin. The corresponding values reported for EB-SPAN are $\sim$ 0.8 states/(eV two-rings) and 0.02 spin/two-rings for the density of states and Curie spin concentration, respectively [2].

The EPR results are consistent with the DC conductivity data within the quasi 1-D VRH model. For the number of nearest neighbor chains equal to 4, $T_0^{LEB-SPAN}/T_0^{EB-SPAN}$ is deter-

mined to be 0.65 from conductivity data and $N(\epsilon_F)^{EB-SPAN}/N(\epsilon_F)^{LEB-SPAN}$ to be 0.78 from EPR data. Thus $(\alpha^{-1})^{LEB-SPAN}/(\alpha^{-1})^{EB-SPAN} \sim 1.0$, establishing that the LEB-SPAN and EB-SPAN results are self-consistent.

pH-dependence of conductivity

Since LEB-SPAN has a higher S/N ratio than EB-SPAN, it is of interest to compare the pH-dependence of their conductivities. We plot σ_{dc}(pH) of LEB-SPAN with those of EB-SPAN and PAN-HCl in Fig. 8. It is clear that for LEB-SPAN σ_{dc} is essentially pH-independent in the available buffer range of pH = 0 to 12 (the variation in σ_{dc} is less than a factor of three). In contrast, for EB-SPAN σ_{dc} drops 5 orders of magnitude from pH = 7.5 to 9 and for PAN-HCl σ_{dc} dropped more than ten orders of magnitude in the region of pH = 2 to 4. This striking difference arises from a greater concentration of sulfonic acid groups attached to the polyaniline backbone in LEB-SPAN. Also, the doping strength of protons from the sulfonic acid groups on the imine nitrogen atoms may be enhanced by the formation of "$-C_2NHOS-$" 6-member ring complexes. As a consequence, these doped imines are more difficult to dedope. Even after exchange of protons with cations such as Li^+ the 6-member-ring conformation may still exist. Thus these imines may still be doped by weaker metal cation Lewis acids. Therefore the samples treated with alkaline aqueous solutions are still highly conducting. The cation size or equivalently in this case, the strength of the Lewis acid used in the buffers, certainly has some effect on conductivity, but it appears to be minimal. This might be explained by: (1) the cation exchange equilibrium position being shifted to a much higher pH due to the presence of an increased concentration of sulfonic acid groups and/or larger cations used in the buffer solution; (2) the effective acid strength of small cations as Li^+ being closer to that of a proton due to complexation.

pH-dependence of $E_{1/2}$ in cyclic voltammogram

The cyclic voltammograms of LEB-SPAN in pH = 1 and pH = 2 buffer solutions are shown in Fig. 9. The half-wave potentials [40], $E_{1/2}$, of LEB-SPAN as a function of pH are plotted in Fig. 10. Each of the half wave potential plots can be fit as a sum of two linear regions. The lower pH regions are the major ones which can be represented as

$$E_{1/2,\,i} = E^{o}_{1/2,\,i} + k_i \cdot pH, \quad i = 1,\ 2, \tag{3}$$

where $E_{1/2,\,i}$ and $E^{o}_{1/2,\,i}$ are the half-wave potential at arbitrary pH and at pH = 0, respectively;

$i = 1$ and 2 denote the first and second oxidation wave, respectively. For $i = 1$ and 2, the half-wave potential data deviate from linear behavior at pH $\geq$ 5 and pH $\geq$ 6, respectively. The plots in lower pH region fit to k_i = -59 mV/pH, representing the reversible behavior of electrochemical oxidation processes, while the plots in higher pH region fit to k_i = -118 mV/pH, representing the hydrolysis process (*vide infra*). A pair of linear $E_{1/2}$ *vs.* pH plots earlier reported for EB-SPAN [2] has a different set of slopes with k_1 = -59 mV/pH and k_2 = -118 mV/pH [2]. The pH dependence of $E_{1/2,\,i}$ for parent polyaniline with $k_1 \sim 0$ mV/pH and $k_2 \sim$ -118 mV/pH [17-20] differs dramatically from that of LEB-SPAN (both k_1 and $k_2 \sim$ -59 mV/pH).

The $E_{1/2}$ *vs* pH plots for LEB-SPAN have some new features as compared to plots for EB-SPAN. For example, at pH = 0, the $E_{1/2,\,1}$ value is larger while $E_{1/2,\,2}$ value is smaller for LEB-SPAN than the corresponding value for EB-SPAN [2]. This is in accord with the suggestion made by Yue *et al* that the reduced separation of the two peaks for EB-SPAN as compared to EB could be a consequence of steric effects associated with the bulky sulfonic acid substituent [2] and a higher S/N ratio. An alternative interpretation is that the sulfonic acid groups (strong electron withdrawing groups (EWGs)), attached to the phenyl rings lower the energy level of the valence band or the highest occupied molecular orbital in the polymer molecule increasing the band gap between the conduction and valence bands [29]. Therefore more energy is needed to remove (ionize) an electron from the polymer chain and consequently $E_{1/2,\,1}$ increases. The reduced $E_{1/2,\,2}$ value could be attributed to the effect of the lowered energy of transition state (similar to *Anomeric Effect* [29]). In the transition state, the non-bonding atomic orbital (in which a lone pair of electrons resides) of the oxygen atom of the sulfonic acid group could overlap with the empty p-orbital (one electron is being removed) of the nearby nitrogen atom to form a 5-member ring complex of lower energy than an open chain transition state. In other words, the energy of the transition state is lowered to yield a smaller $E_{1/2,\,2}$. Therefore the smaller separation between peaks in LEB-SPAN could indicate a greater density of sulfonic acid groups attached to phenyl rings in LEB-SPAN. Noted, however, that recent quantum chemistry calculations of EB-SPAN and emeraldine salt in the polaron lattice form indicate little difference between their HOMO-LUMO gaps [41].

The apparent deviation of $E_{1/2}$ *vs.* pH from a straight line behavior pH $\geq$ 5 may be attributed to the irreversible degradation of polymer chains by hydrolysis. When an amine moiety is

oxidized to the iminium cation, some positive charge density will be induced on the adjacent carbon atoms which is readily attacked by hydroxide anions and subsequently hydrolyzed [8, 17, 42, 43]. The higher the pH (or concentration of hydroxide anion) and/or the scan potential, the more severe this type of nucleophilic substitution reaction. The hydrolysis mechanism at the second oxidation wave is schematically illustrated in *Scheme 9, vide infra.* The quantitative representation of this process is given below.

Models for Electrochemical Redox Processes

First as a simplified picture of the electrochemical oxidation processes in polyaniline, we propose a quasi-random oxidation model, similar to the statistical "Box Model" for polarons and bipolarons on chains in polypyrrole, proposed by Genoud *et al* [44] and Devreux [45]. This model provides a basis for understanding the pH-dependent CV and *in situ* EPR data (i.e., the hydrolysis effects and the large ratio ($2 \sim 3$) of the EPR intensity at the first CV oxidation wave (LEB $\longrightarrow$ ES) to that of the second CV oxidation wave (ES $\longrightarrow$ PNB) [18, 19, 21-25]. This model assumes that the oxidation of amine sites along the LEB polymer backbone occurs randomly. The effects of Coulomb repulsion between the charged oxidation sites (assumed localized) are examined. In addition, the role of a polaron lattice (Pauli susceptibility *vs.* Curie susceptibility) on the simulation of the reported *in situ* EPR signal is studied. Based on this schematic microscopic picture, we propose a set of half electrode reactions for pH-dependent electrochemical oxidation processes, predict the slopes of their $E_{1/2,\,i}$ *vs.* pH plots from the Nernst equation, and compare those predicted values with the experimentally determined slopes.

Quasi-random oxidation model: Several assumptions are made in this model: (1) At the early stage of the oxidation process the polymer repeat units are oxidized to form polarons; (2) Coulomb repulsion favors the configurations with the largest separation of charged polarons (i.e., the formation of doubly charged bipolarons is not favored at the early stage); (3) Adjacent pairs of polarons when they do occur have zero magnetic susceptibility (caused by strong anti-ferromagnetic coupling, as expected for the spins on nitrogen sites interacting through the para positions of benzene rings [46], or by formation of a bipolaron-like doubly charged spinless quinoid units, or by formation of spinless neutral quinoid units as the result of deprotonation of charged bipolarons).

The mutual relationships between the Reduced Substituted Aniline ring unit (RSA) and the

Oxidized Substituted Aniline ring unit (OSA) (including its cation radical form (OSA_+) and its deprotonated neutral radical form (OSA_n)) are given in *Scheme 4* (I). These relations are presented in symbolic form in *Scheme 4* (II) to enable an easier description of *Scheme 5* below.

In *Scheme 5*, we illustrate the oxidation processes schematically in terms of the symbolic polymer repeat units defined in *Scheme 4* and at the bottom of *Scheme 5*. It is impossible to present all of the possible configurations and paths in *Scheme 5*, therefore we illustrate only the random oxidation of RSAs and the origin of the large ratio of the intensity of the first peak over the second one of the *in situ* EPR spectra. We note where paths and configurations are omitted with symbol "..." in *Scheme 5*. The simulation presented below does include all possible configurations.

In *Scheme 5*, RSAs in a substituted LEB polymer chain (I), represented as N repeat segments composed of 8 RSA units each, is shown being oxidized to the charged radical state OSA_+ along configuration (II) *via* path 1. Here we explicitly write out configuration (II) which has the smallest Coulomb repulsion.

Potentially there are three paths by which the polymer chain (II) can be further oxidized to polymer chain (III X) (X = A, B, C) (note that (III A) and (III C) are equivalent). The shape of the *in situ* EPR and CV spectra will be shown to be dependent upon the paths taken. First it is assumed that (II) is oxidized only through the "conventional" paths, i. e., (II) $\longrightarrow$ (III A) or (II) $\longrightarrow$ (III C). In the model of Huang *et al* [17], adjacent amine nitrogen atoms always are paired up during the oxidation reaction, which implies that the two nitrogen atoms are oxidized either simultaneously or consecutively in the oxidation process. Thus the oxidized polymer ((III A) or (III C)) obtained through this path contains only doubly charged spinless bipolarons, resulting in a zero intensity in the *in situ* EPR/CV spectra, contradicting the reported nonzero minimum *in situ* EPR intensity [18, 19, 21-25]. Therefore other paths contributing to spin signal are present.

We now discuss the oxidation of polymer from configuration (II) to (III B) through path 2b. The oxidation *via* path 2b occurs readily because (1) the amines undergoing oxidation are less affected by the induction effect of the positive charge already present (the cations are further separated compared to those produced following the "conventional" path) and (2) the formation of a polaron lattice further lowers the energy. In fact, the thermodynamic stability

of configuration (III B) over that of configuration (III A) or (III C) (a bipolaron lattice) has been implied in the proposed bipolaron-polaron phase transition [47]. More importantly, this configuration would contribute to the magnetic susceptibility, supporting its central role in the *in situ* EPR signal recorded during a CV potential scan.

The configuration (III B) in *Scheme 5*, the oxidation product of polymer chain (II) along path 2b, is a representative of configurations which, differing from those of (III A) and (III C), have a positive contribution to the magnetic susceptibility. In other words, at this oxidation stage the Pauli and the Curie spins are mixed together with their weighting factors as a function of the scan potential and the number of polarons centered on alternating sites.

Paths 3x and 4x (x = a, b, c) show stepwise oxidation of the substituted ES to PNB. The experimental EPR peak intensity during the second oxidation wave is smaller than during the first one. Based on the *quasi-random oxidation model* we are able to roughly estimate the ratio of intensities of the two EPR peaks.

When estimating the spin concentration for oxidation stages indicated in *Scheme 5*, we assume, for simplicity, equal probability for all possible parallel paths. Also note that we use a localized description rather than a delocalized picture to represent a polaron lattice [47, 48]. If the EPR signal at the first wave is assumed to arise from configuration (II), then the total spin will be N (i.e. 2N contributions of spin one-half), and the other similar configurations will also have a total spin of $\sim$ N. In contrast, if the EPR signal at the second oxidation wave is assumed to derive from the configurations shown in (IV), weighted by the probability of their occurrences, then the total spin will be reduced. The average spin is determined as (5/9)N, from 8 configurations of spin zero (four (IV A)s from path 3a$'$ and 3c$'$ each) and 10 configurations of spin one (6 (IV B)s from path 3b and two from path 3a and 3c each), i.e. $(8\times0 + 10\times1)N/18 = (5/9)N$. This yields an EPR integrated intensity ratio between the first and the second oxidation wave of approximately $N/[(5/9)N] = 1.8$, in agreement with the reported experimental ratio $\sim$ 2.

Simulations [49] based on the *quasi-random oxidation model* assumptions have been carried out for chain lengths up to a 1000 C_6N units including the contribution for a polaron lattice as described below. The polymer spin concentration contributed by configuration (III B) would be over-estimated if the polaron lattice were not considered. The Pauli susceptibility is $\mu_B^2 N(\epsilon_F)$ (the

density of states, $N(\epsilon_F)$, is measured from both the conductivity and the magnetic susceptibility experiments). To prevent the over-estimation of the spins from configuration (III B) and in recognition of the zero spin contribution of doubly oxidized tetramers of emeraldine salt [50] and the Pauli susceptibility of octamers [51] and longer lengths [52] of emeraldine salt, we adopt the following counting scheme. The spin contribution of lengths of six or more polarons centered on alternating sites (i.e., hexamers or longer) are counted as Pauli spin and set its value to $\frac{1}{l^2} + 0.001$, where 'l' is the length of "Pauli segment". For example, we count the spin of the 8-ring segment in configuration (III B) of *Scheme 5*, as $0.001 + 1/8^2$. While we count isolated polarons (separated by more than two ring units) as Curie spins (e.g. 2N times spin one-half as in the configuration (II) of *Scheme 5*) and count two adjacent polarons as spin zero (e.g. zero spin for configuration (V) in *Scheme 5*). These counting schemes are exemplified in Table 1.

In the simulation, we varied the ratio of the Coulomb repulsion between two polarons on the nearest neighbor sites (U_1) to that on the next nearest neighbor sites (U_2) and found the best fit to be $U_1/U_2 \sim 40$. This implies very strong screening as the charged polarons separate. The simulation result is plotted in Fig. 11. The ratio of the peaks of the spin concentration in Fig. 11 converges to ~ 2.2 with a minimum susceptibility at $\sim 1/10$ of the first peak value, similar to the experimental value.

Based on *Scheme 5* and the simulation result in Fig. 11, we present a qualitative description of the reported *in situ* EPR signals [18, 19, 21-25] as a function of the CV potential. Configuration (I) represents a polymer chain in the LEB oxidation state, which has zero spin, corresponding to the stage before the threshold of the first oxidation wave. Through path 1, LEB is oxidized to yield configuration (II), a representative of configurations with predominantly isolated polarons (Curie spins) along the chain (namely, protoemeraldine [53]), which has the largest possible EPR signal within this model. Upon oxidation of the protoemeraldine, spinless emeraldine (paths 2a and 2c, yielding either doubly charged spinless bipolarons, or, after deprotonation, spinless imine units) and spin containing emeraldine salt (the Curie spin as (III B) literally indicated and the Pauli spin, both implied through path 2b) are formed. This oxidation stage corresponds to a non zero EPR intensity as reported in the region between the peaks of the first and the second oxidation waves. As the oxidation continues through path 3x, the polymer chain is oxidized further to nigraniline [53], which is suggested to correspond to the second peak

of the *in situ* EPR signal. At this potential the EPR intensity is one-half of that at the first maximum. Further oxidation of the polymer leads to the highest oxidation state of polyaniline, pernigraniline, which is spinless. It is noted that neither protoemeraldine nor nigraniline are separable oxidation state of the chemically oxidized polymer (which only have leucoemeraldine, emeraldine, and pernigraniline as discrete oxidation states [54]).

The other evidence which supports this model comes from the consistency of the predicted and the experimentally determined ratio of two *in situ* EPR peaks of hydrolyzed samples. For example, if hydrolysis occurs during the multiple potential scan in the *in situ* CV and associated EPR experiment, and the sample film is continuously degraded into smaller and smaller fragments, say, segments with lengths less than 8 ring units, then the ratio of the intensities of the *in situ* EPR peaks corresponding to the first and the second oxidation waves of CV experiment will increase dramatically. Our model shows that oligomers with lengths less than 5 do not contribute to the second peak of the *in situ* EPR spectrum. Indeed, the ratio of the EPR intensities at the first and at the second oxidation waves reported by Lapkowski *et al* [24] is ~ 5 when the "central" peak (signature of hydrolysis [42]) is present. It is worthwhile to note that the presence of the defect states of base forms of polyaniline and its derivatives is a natural outcome of the *quasi-random oxidation model.*

In summary, the statistical *quasi-random oxidation model* of the electrochemical oxidation of LEB to PNB *via* multiple paths accounts for the variation of the *in situ* EPR intensity, in contrast to the conventional (consecutive or simultaneous) oxidation model [17].

Model for pH-dependence of oxidation reactions: The dependence of the oxidation potential, E, of a reversible half-electrode reaction,

$$R \longrightarrow O + ne + mH^+, \tag{4}$$

can be described by the Nernst equation,

$$\begin{aligned} E &= E^o + \frac{RT}{nF} ln[H^+]^m \\ &= E^o - 0.059\frac{m}{n}pH, \quad at\ 25^o\ C, \end{aligned} \tag{5}$$

where R represents the species at lower oxidation state and O the species at higher oxidation state, m and n are the coefficients for electrons and protons involved in the reaction (4), respec-

tively. The standard potential, E° in equation (5), is equivalent to $E^\circ_{1/2}$, the half wave potential [40] in a cyclic voltammogram.

In order to interpret the complicated phenomena related to the electrochemical redox processes of PANI and its derivatives, some general electrochemical processes are proposed in *Schemes 3, 6-9*. It is assumed that these proposed electrochemical processes are reversible enabling application of the Nernst equation. Because the time scale of the redox process (scan rate of 10 mV/sec was typical) in cyclic voltammetry is $\sim$ 50 s, quasi equilibrium conditions are assumed and hence a steady state treatment [22] is valid. As a consequence, we can calculate and compare the calculated slopes with the experimental ones.

In *Scheme 3* (I), the symbols used in *Schemes 3, 6-9* are defined. "A" in "A_f" represents a substituent, which could be a hydrogen atom, or a "$-SO_3H$" group, or any other substituent. The subscript "f" denotes a number (a fraction or a whole number, taking values from 0 to 4, representing number of "A" statistically attached to a phenyl ring). M^+ can be a proton, or a metal cation (such as K^+ from the supporting electrolyte, say, from 1 M KCl in a pH $>$ 1 solution). The "spring-like" symbol defined in *Scheme 3* (I) represents a substituted phenyl ring that does not change during electrochemical processes.

Scheme 3 (II) schematically illustrates the resonance of a polaron between two adjacent nitrogen sites, (**3C**) and (**3D**), through an intermediate state, (**3CD**), *via* an internal redox reaction. Though positive polarons are thought to be more delocalized than indicated here, their resonance between two adjacent sites will proceed in the same manner.

Scheme 6 describes the general equilibria of redox reactions and their related protonation-deprotonation reactions. $K^j_{p,\,i}$ and $K^j_{d,\,i}$ are the equilibrium constants for the protonation and deprotonation reactions for i'th reagent at j'th oxidation level, respectively. $k^j_{proto_i}$ and $k^j_{deproto_i}$ are protonation and deprotonation rate constants for i'th reagent at j'th oxidation level, respectively. In *Scheme 6* (I), a general description of sequential protonation equilibria of the polymer backbone at arbitrary oxidation level (i.e., substituted LEB, or EB, or PNB) is given. In *Scheme 6* (II), general oxidation processes, where radical cations are formed followed by sequential deprotonation-protonation equilibria, are shown. Of course the effect of the Coulomb repulsion will modify the individual equilibrium constants.

Scheme 7 shows the proposed oxidation processes in less acidic media, where the deprotona-

tion of the oxidation product occurs completely. In *Scheme 7* (I) and (II), the oxidation of the substituted LEB (**3B**) to the substituted EB (**7E**), and then to the substituted PNB (**7F**) is given. As each of these steps involves the simultaneous removal of one electron and one proton, the slope of the half wave potential *vs* pH for each of these processes is $\sim$ -59 mV/pH.

Scheme 8, in contrast to *Scheme 7*, illustrates how the most probable oxidation processes occur in a very acidic media where both the starting polymer and the oxidation products are protonated to a considerable extent. For the emeraldine oxidation state, the deprotonated form is in equilibrium with the protonated form (or the usual emeraldine salt form, etc.), with their ratio affected by pH. *Scheme 8* (I) shows that a protonated amine is oxidized first. Then the product (**8H**) is deprotonated because that the two positive charges experience a strong Coulomb repulsion. Therefore the half-wave potential *vs* pH is $\sim$ -59 mV/pH. On the other hand, the slope of the oxidation potential *vs* pH for *Scheme 8* (II) is likely between 0 and -59 mV/pH, which can be rationalized as that at higher potential and lower pH (say, 1 M HCl), the accumulating polarons centered on adjacent sites combine to yield doubly charged polaron 'pairs' (**8I**), with strong anti-ferromagnetic coupling (suppressing the measured spin) [22, 46]. These polaron 'pair' sites are eventually deprotonated to form the quinoid counterpart (**7F**) in the presence of an applied electric field (see *Scheme 8* (III)).

Scheme 9 shows the mechanism for electrochemical oxidation-hydrolysis reaction. In *Scheme 9* (I), the oxidation-hydrolysis of EB in less acidic media is shown and slope is $\sim$ -118 mV/pH. While in *Scheme 9* (II) the oxidation-hydrolysis of LEB in a very acidic media is described and it is seen that the slope is only $\sim$ -59 mV/pH.

In short, three types of slopes are obtained: (1) For the processes involving equilibria of protonation-deprotonation of the species during the oxidation process, the slopes are between zero and -59 mV/pH, which may correspond to the slightly decreased slope at the beginning portion of our plot (see Fig. 10); (2) for the process with m/n = 1 (see equation (5)) the slope is -59 mV/pH, which is clearly observed in the middle portion of our plot; (3) for the processes where oxidation-hydrolysis occurs (m/n = 1/2), the slope is -118 mV/pH. The portions of our data at higher pH yield a slope of $\sim$ -118 mV/pH, providing evidence for hydrolysis. This is supported with the observation of the irreversibility associated with the first and second oxidation wave: we observed a third set of peaks, the so called "central peak" [55] (signature of

hydrolysis [42]), at $\sim$ 0.4 volts (*vs* Ag/AgCl) on the CV spectrum of an LEB-SPAN film coated electrode in pH = 1 solvent for scan potential < 0.7 V. The film deliberately earlier had been subjected to CV (for scan potential < 0.35 V) in electrolyte of pH = 6. As shown in *Scheme 9* (II), at low pH, hydrolysis could also occur with a slope of -59 mV/pH, the same slope as observed during the usual normal redox process of PANI and its derivatives. We have observed evidence for the occurrence of hydrolysis at low pH with the first and the second set of oxidation waves of the CV rapidly merging into a new set of "central" peaks when the upper limit of the scan potential was set to 1.4 volts for a LEB-SPAN electrode at pH = 1.

The differences in electrochemical behavior between LEB-SPAN and the other forms of PANI can be understood as following. First, the reduced hydrolysis for LEB-SPAN at pH < 5 is suggested to be the consequence of having more substituents such as sulfonic acid groups; these groups could partially shield the carbine [29] from being attacked by anions, e.g., hydroxide ions). A second note concerns the difference in the slope of oxidation potential *vs* pH for the SPAN samples as compared with the parent polyaniline. For parent polyaniline, the corresponding two half-electrode processes are: (1) **(3B)** $\longrightarrow$ **(3C)**, with $k_1 \sim 0$; (2) **(3C)** $\longrightarrow$ **(8I)** $\longrightarrow$ **(7F)**, yielding $k_2 \sim$ -118 mV/pH. On the other hand, LEB-SPAN has bulky substituents which are EWG's in nature, having the following consequences: (1) EWGs are withdrawing some electron density from the ring therefore destabilizing the polaron or doubly charged bipolaron (in other words, deprotonation occur more readily); (2) Bulky substituents open more and larger channels for ions to diffuse in or out, which makes the local pH closer to the bulk pH. Therefore LEB-SPAN will have an improved dynamic response to the bulk pH, yielding both k_1 and $k_2 \sim$ -59 mV/pH.

Summary

The element chemical analyses, consistent with XPS analyses, of LEB-SPAN show sulfonation levels as high as S/N $\sim$ 0.75 with high yield ($\sim$ 0.7). FTIR and UV-Vis, CV spectra, and pH-dependence of conductivity are consistent with the higher S/N ratio. EPR and DC conductivity data are self-consistent, showing that LEB-SPAN has a higher conductivity with a weaker temperature dependence as compared to EB-SPAN. The conductivity of LEB-SPAN persists to

much higher pH than that of parent emeraldine salt and even EB-SPAN.

We have proposed a statistical *quasi-random oxidation model* for the electrochemical redox processes of PANI and its derivatives. Based on this model, we quantitatively simulated the *in situ* EPR/CV spectrum, rationalized the different behavor between the pH-dependent CV experiments of SPAN and PANI, and interpreted the hydrolysis related phenomena during the electrochemical redox reactions.

Acknowledgement

This work has been supported in part by the Office of Naval Research.

References

[1] Yue, J.; Epstein, A. J. *J. Am. Chem. Soc.* **1990**, *112*, 2800-1.

[2] Yue, J.; Wang, A. H.; Cromack, K. R.; Epstein, A. J.; MacDiarmid, A. G. *J. Am. Chem. Soc.* **1991**, *113*, 2665-71.

[3] Yue, J.; Gordon, G.; Epstein, A. J. *Polymer* **1992**, *33*, 4409-18.

[4] (a) Yue, J.; Epstein, A. J.; Zhong, Z.; Gallagher, P. K.; MacDiamid, A. G. *Synth. Met.*, **1991**, *41*, 765-8; (b) Tsai, T.-C.; Tree, D. A.; High, M. S. *Ind. Eng. Chem. Res.*, **1994**, *33*, 2600-6.

[5] (a) Barbero, C.; Miras, M. C.; Schnyder, B.; Haas, O.; Koetz, R. *J. Matter. Chem.*, **1994**, *4*, 1775-83; (b) Barbero, C.; Miras, M.C.; Kotz, R.; Haas, O. in *Lithium Batteries* (Proc. Electrochem. Soc.) **1994**, *94-4*, 281-92; (c) Barbero, C.; Miras, M. C.; Koetz, R.; Haas, O. *Synth. Met.*, **1993**, *55*, 1539-44.

[6] Zhang, G.; Gong, K. *Yingyong Kexue Xuebao*, **1994**, *12*, 92-4.

[7] (a) Onoda, M.; Yoshino, K. *J. Appl. Phys.*, **1995**, *78*, 4456-62; (b) Onoda, M.; Yoshino, K. *Jpn. J. Appl. Phys., Part 2*, **1995**, *34 (2B)*, L260-L263; (c) Ferreira, M.; Rubner, M. F. *Macromolecules*, **1995**, *28*, 7107-14. *Jpn. J. Appl. Phys., Part 2*, **1995**, *34*, L260-L263.

[8] Yue, J.; Epstein, A. J. *J. Chem. Soc., Chem. Commun.* **1992**, *21*, 1540-42.

[9] Kawai, T.; Mizobuchi, H.; Yamasaki, N.; Araki, H.; Yoshino, K. *Jpn. J. Appl. Phys., Part 2*, **1994**, *33*, L357-L360.

[10] (a) Namiki, T.; Yano, E.; Watabe, K.; Igarashi, Y.; Kuramitsu, Y.; Maruyama, T.; Yano, K.; Nakamura, T.; Shimizu, S.; Saito, T. *Patent*, Patent information: JP 07179754 A2 950718 Heisei; (b) Watable, K.; Yoneda, Y.; Maruyama, T.; Yano, K.; Nakamura, T.; Shimizu, S.; Saito, T. *Patent*, Patent information: JP 06003813 A2 940114 Heisei.

[11] Shimizu, S.; Saitoh, T.; Natamura, T. *Patent*, Patent information: DE 4244359 A1 930701.

[12] (a) MacDiarmid, A. G.; Epstein, A. J. *Synth. Met.* **1994**, *65*, 103-116; (b) MacDiarmid, A. G.; Epstein, A. J. *Trans., 2nd Congresso Brazileiro de Polimeros*, São Paulo, Brazil, Oct. **1993** *5-8*, 544-51; (c) Min, Y.; MacDiarmid, A. G.; Epstein, A. J. *Polymer Prepr.*, **1993**, 231-2; (d) MacDiarmid, A. G.; Epstein, A. J. *Synth. Met.*, **1995**, *69*, 85-92.

[13] (a) Cao, Y.; Smith, P.; Heeger, A. J. *Synth. Met.*, **1992**, *48*, 91-7; (b) Cao, Y.; Heeger, A. J.; *Synth. Met.*, **1993**, *52*, 193-200; (c) Cao., Y.; Treacy, G. M.; Smith, P.; Heeger, A. J. *Appl. Phys. Lett.*, **1992**, *60*, 2711-13; (d) Cao, Y. Smith, P. *Polymer*, **1993**, *34*, 3139-43.

[14] Patil, A. D.; Ikenoue, Y.; Basescu, N.; Colaneri, N.; Chen, J.; Wudl, F.; Heeger, A. J. *Synth. Met.*, **1987**, *20*, 151-9.

[15] MacDiarmid, A. G.; Epstein, A. J. in *Front. Polym. Adv. Mater.*, Proc. Int. Conf., *2*; Plenum Press: New York, 1994; pp251-61.

[16] (a) Tsutsumi, H.; Fukuzawa, S.; Ishikawa, M.; Morita, Y. *J. Electrochem. Soc.*, **1995**, *142*, L168-L170; (b) Hwang, K.; Kim, J. S.; Kong, M. J. *Synth. Met.*, **1995**, *71*, 2201-2; (c) Oyama, N.; Tatsuma, T.; Sato, T.; Sotomura, T. *Nature*, **1995**, *373*, 598-600; (d) Morita, M.; Miyazaki, S.; Ishikawa, M.; Matsuda, Y.; Tajima, H.; Adachi, K.; Anan, F. *J. Electrochem. Soc.*, **1995**, *142*, L3-L5.

[17] Huang, W.; Humphrey, B. D.; MacDiarmid, A. G. *J. Chem. Soc., Faraday Trans.* **1986**, *82*, 2385-400.

[18] Wolf, J. F.; Forbes, C. E.; Gould, S.; Shacklette, L. W. *J. Electrochem. Soc.* **1989**, *136*, 2887-91.

[19] Glarum, S. H.; Marshall, J. H. *J. Phys. Chem.* **1988**, *92*, 4210-7.

[20] Focke, W. W.; Wnek, G. E. *J. Electroanal. Chem.* **1988**, *256*, 343-52.

[21] Villeret, B.; Nechtschein, M. *Phys. Rev. Lett.* **1989**, *63*, 1285-7.

[22] Tang, J.; Allendoerfer, R. D.; Osteryoung, R. A. *J. Phys. Chem.* **1992**, *96*, 3531-6.

[23] Ohsawa, T.; Kabata, T.; Kimura, O.; Onoda, M.; Yoshino, K. *Jpn J. of Appl. Phys.* **1989**, *28*, 996-9.

[24] Lapkowski, M.; Geniés, E. M. *J. Electroanal. Chem.* **1990**, *279*, 157-68.

[25] Kruszka, J.; Nechtschein, M.; Santier, C. *Rev. Sci. Instrum.* **1991**, *62*, 695-9.

[26] Wei, X.-L.; Epstein, A. J. *Synth. Met.*, in press.

[27] MacDiarmid, A. G.; Chiang, J.; Richter, A. F.; Somasiri, N. D. L.; Epstein, A. J. In *Conducting Polymers*, Riedel, D., Alcacer, L., Eds.; Dordrecht: Holland, 1987; pp97-118.

[28] Zuo, F.; Angelopoulos, A.; MacDiarmid, A. G.; Epstein, A. J. *Phys. Rev. B.* **1987**, *36*, 3475-8.

[29] Carey, F. A.; Sundberg, R. J. *Adavanced Organic Chemistry, Part A: Structure and Mechanisms*; Plenum Press: New York and London, 1990.

[30] Colthup, N. B.; Daly, L. H.; Wiberley, S. E. *Introduction to Infrared and Raman Spectroscopy*; Academic Press: Harcourt Brace Jovanovich, 1990.

[31] Ginder, J. M.; Epstein, A. J.; MacDiarmid, A. G. *Solid State Commun.* **1989**, *72*, 987-90.

[32] Ginder, J. M.; Epstein, A. J. *Phys. Rev. B.* **1990**, *41*, 10674-85.

[33] Epstein, A. J.; Ginder, J. M.; Zuo, F.; Bigelow, R. W.; Woo, H.-S.; Tanner, D. B.; Richter, A. F.; Huang, W.-S.; MacDiarmid, A. G. *Synth. Met.* **1987**, *18*, 303-9.

[34] Wang, Z. H.; Scherr, E. M.; MacDiarmid, A. G.; Epstein, A. J. *Phys. Rev. B.* **1992**, *45*, 4190-202.

[35] Mott, N. F.; Davis, E. *Electronic Processes in Non-Crystalline Materials*; Clarendonm: Oxford, 1979.

[36] Goldberg, I. B.; Gowe, H. R; Newman, P. R.; Heeger, A. J; MacDiarmid, A. G. *J. Chem. Phys.* **1979**, *70*, 1132-6.

[37] Scott, J. C.; Pflunger, P.; Krounbi, M. T.; Street, G. B. *Phys. Rev. B.* **1983**, *28*, 2140-5.

[38] Javadi, H. H. S.; Laversanne, R.; Epstein, A. J.; Kohli, R. K.; Scherr, E. M.; MacDiarmid, A. G. *Synth. Met.* **1989**, *29*, E439-E444.

[39] Carrington, A.; McLachlan, A. D., Ed. *Introduction to Magnetic Resonance*; Chapman and Hall: London, 1967.

[40] Bard, A. J.; Faulkner, L. R. *Electrochemical Methods: Fundamentals and Applications*; John Willey & Sons Press: New York, 1980.

[41] Libert, L.; Brédas, J. L. To be published.

[42] Rodrigue, D.; Snauwaert, P.; Demaret, X.; Riga, J.; Verbist, J. J. *Synth. Met.* **1991**, *41-43*, 769-73.

[43] McManus, P.; Cushman, R. J.; Yang, S. C. *J. Phys. Chem.* **1987**, *91*, 744-7.

[44] Genoud, F.; Guglielmi, M.; Nechtschein, M.; Genies, E.; Salmon, M. *Phys. Rev. Lett.* **1985**, *55*, 118-21.

[45] Devreux, F. *Europhys. Lett.* **1986**, *1*, 233-9.

[46] Miller, J. S.; Epstein, A. J. *Angew. Chem. Int. Ed. Engl.* **1994**, *33*, 385-415.

[47] Stafström, S.; Brédas, J. L.; Epstein, A. J.; Woo, H. S.; Tanner, D. B.; Huang, W. S.; MacDiarmid, A. G. *Phys. Rev. Lett.* **1987**, *59*, 1464-7.

[48] Libert, J.; Brédas, J. L.; Epstein, A. J. *Phys. Rev. B.* **1995**, *51*, 5711-24.

[49] Wei, X.-L. *Ph. D. dissertation.*

[50] Javadi, H. H. S.; Treat, S. P.; Ginder, J. M.; Wolf, J. F.; Epstein, A. J. *J. Phys. Chem. Solids* **1990**, *51*, 107-12.

[51] Wudl, F.; Angus, R. O. Jr.; Lu, F. L.; Allemand, P. M.; Vachon, D. J.; Novak, M.; Liu, Z. X.; Heeger, A. J. *J. Am. Chem. Soc.* **1987**, *109*, 3677-84.

[52] Ginder, J. M.; Richter, A. F.; MacDiarmid, A. G.; Epstein,

[53] Green, A. G.; Woodhead, A. E. *J. Chem. Soc.* **1910**, 2388-403.

[54] Chen, S.-A.; Hwang, G.-W. *J. Am. Chem. Soc.* **1994**, *116*, 7939-40. A. J. *Solid. St. Commun.* **1987**, *63*, 97-101.

[55] (a) Sun, Y.; MacDiarmid, A. G.; Epstein, A. J. *J. Chem. Soc., Chem. Commun.* **1990**, *7*, 529-31; (b) MacDiarmid, A. G.; Manohar, S. K.; Masters, J. G.; Sun, Y.; Weiss, H.; Epstein, A. J. *Synth. Met.* **1991**, *41-43*, 621-6.

Figures and Figure captions

Figure 1 FTIR spectra: ——, self doped form of LEB-SPAN in KBr pellet; - - -, self doped form of EB-SPAN in KBr pellet. The spectrum of EB-SPAN was adapted from ref. [3].

Figure 2 FTIR spectra: ——, EB-I in KBr pellet; - - -, ES-I in KBr pellet.

Figure 3 Solution UV-Vis spectra for SPAN base: ——, LEB-SPAN in aqueous 0.1 M NH_4OH, maxima at 312 nm (eV) and 541 nm (eV); - - -, EB-SPAN in aqueous 0.1 M NH_4OH, maxima at 320 nm and 563 nm. Cuvettes used for all of above spectra are from Aldrich Chemical Company (10-mm light path and transparent from 165 nm to 2600 nm). The spectrum of EB-SPAN was adapted from ref. [3].

Figure 4 Temperature dependence of DC conductivity of LEB-SPAN sample plotted as $\log_{10}\sigma$ *vs.* $T^{-1/2}$ (Fit to 1D-VRH model).

Figure 5 Temperature dependence of EPR linewidth for LEB-SPAN: full width at half maxima linewidth FWHM ($\diamond$).

Figure 6 Temperature dependence of g-value for LEB-SPAN sample: g-value at center field of EPR signal of the first derivative spectrum ($\diamond$). The solid line is the the linear fit to the data.

Figure 7 Magnetic susceptibility times temperature versus temperature plot. $N(\epsilon_F)$ was obtained from linear fit to the data ($\cdots$) in the temperature region of (2 K, 250 K).

Figure 8 pH-dependence of DC conductivity at room temperature for LEB-SPAN ($\bullet$), EB-SPAN ($\diamond$), and PAN-HCl ($\triangle$). The data of EB-SPAN and PAN-HCl were adapted from ref. [3].

Figure 9 Cyclic voltammograms of LEB-SPAN in pH = 1.0 (——) and pH = 2.0 (- - -) buffer solution. The scan rate is 50 mV/s and current range is 100 mA.

Figure 10 Half-wave potential, $E_{1/2,\,i}$, of LEB-SPAN sample *vs.* pH plot: The first oxidation potential $E_{1/2,\,1}$ was fit into a straight line with slope = -60 mV/pH while the second oxidation

potential $E_{1/2,\ 2}$ was fit into two segments of straight lines (the slope of line from pH = 1 to pH =5 is -60 mV/pH while that from pH = 5 to pH = 7 is -118 mV/pH). (○) and (●) represent data for one electrode and so do "open" and "filled" (△) for another. The electrodes were prepared with powders of same batch of SPAN.

Figure 11 Simulation result of *in situ* EPR signal intensity as a function of CV scan potential. "•" are the computational data averaged to 500 hundred times.

Table 1 Spin-counting schemes used in the simulation of the *in situ* EPR data.

Case	Configuration of Oxidized Polymer Chain	Type	Spins
A	O R O R O R O R O R O R O R O R	Pauli	$(\frac{1}{16^2} + 0.001)$
B	O R R R R R R R O R O R R R O R	Curie	$4 \times \frac{1}{2}$
C	O O R R R R R R O O R R R R O O	Bipolaron	3×0
D	O O R R O R O R O R O R R R R O	Mixed	$\frac{1}{2} + (\frac{1}{8^2} + 0.001)$

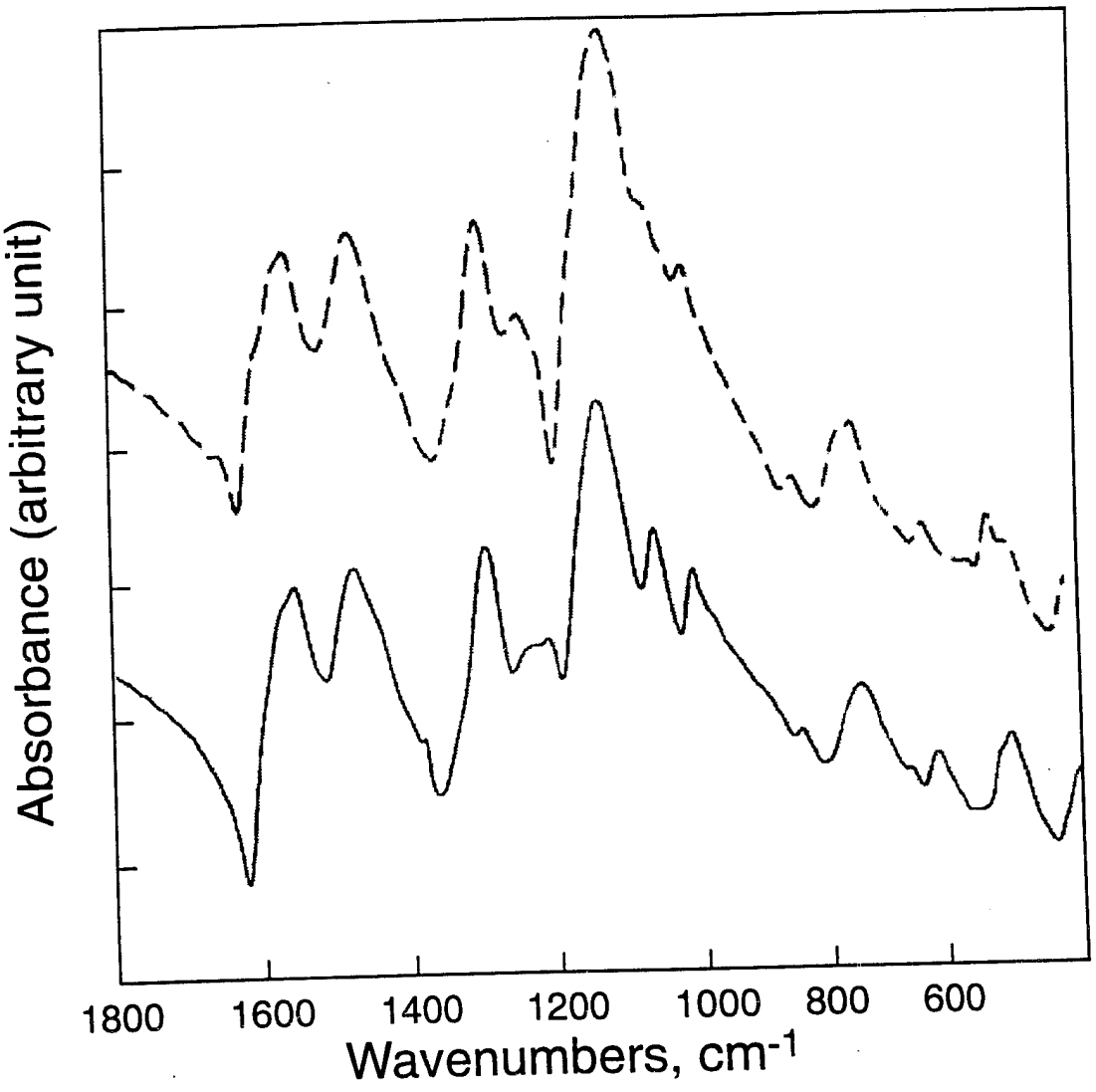

Fig. 1, Wei *et al*

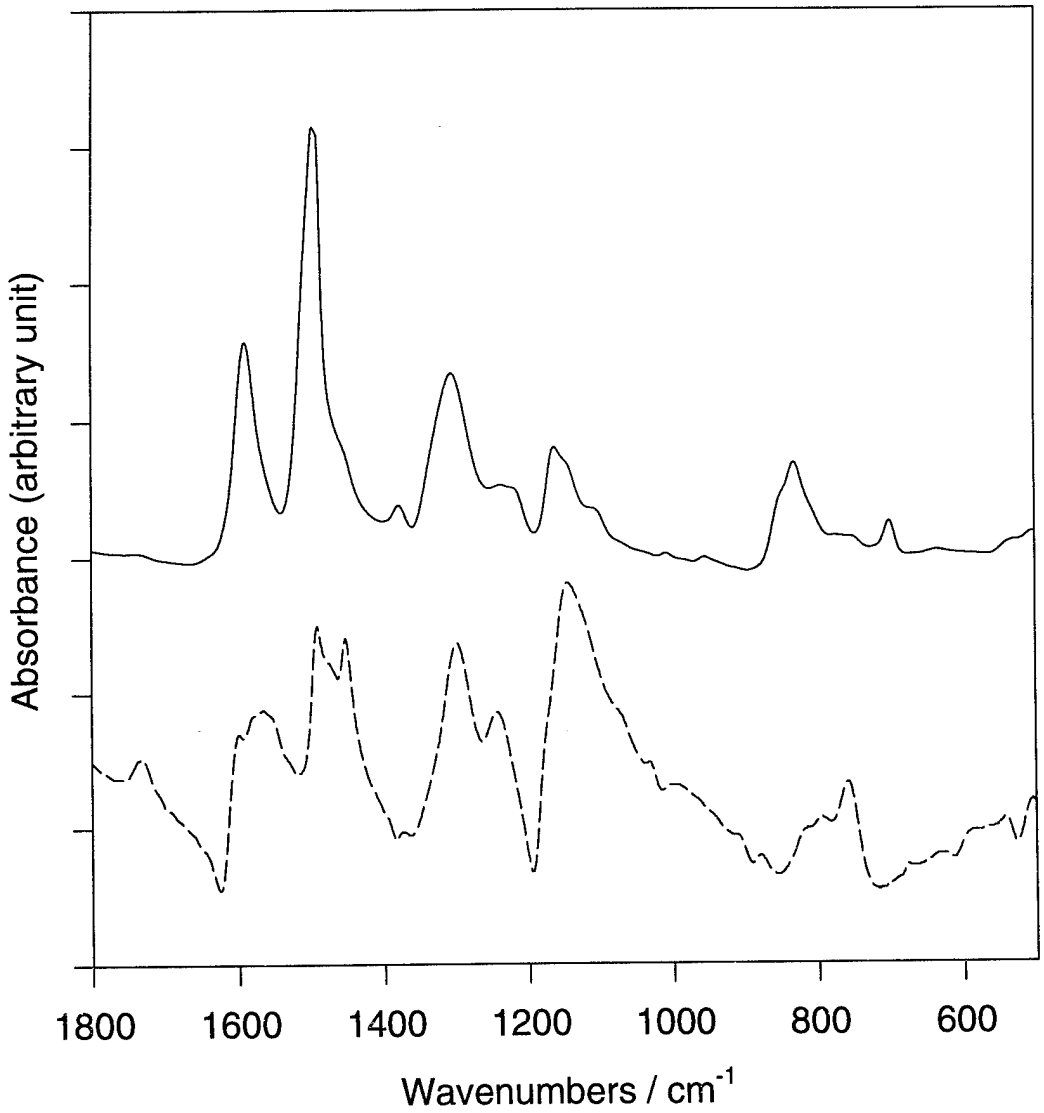

Fig. 2, Wei *et al*

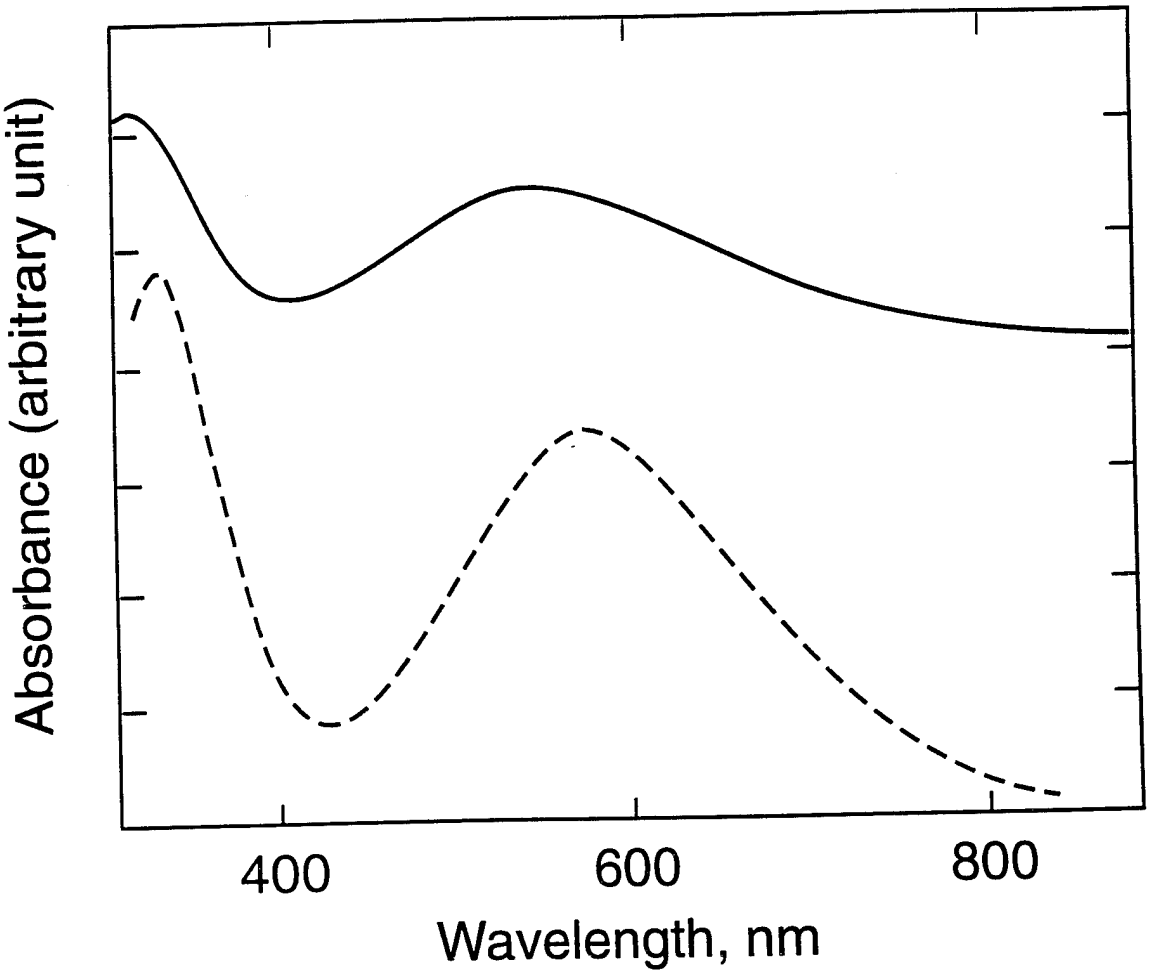

Fig. 3, Wei *et al*

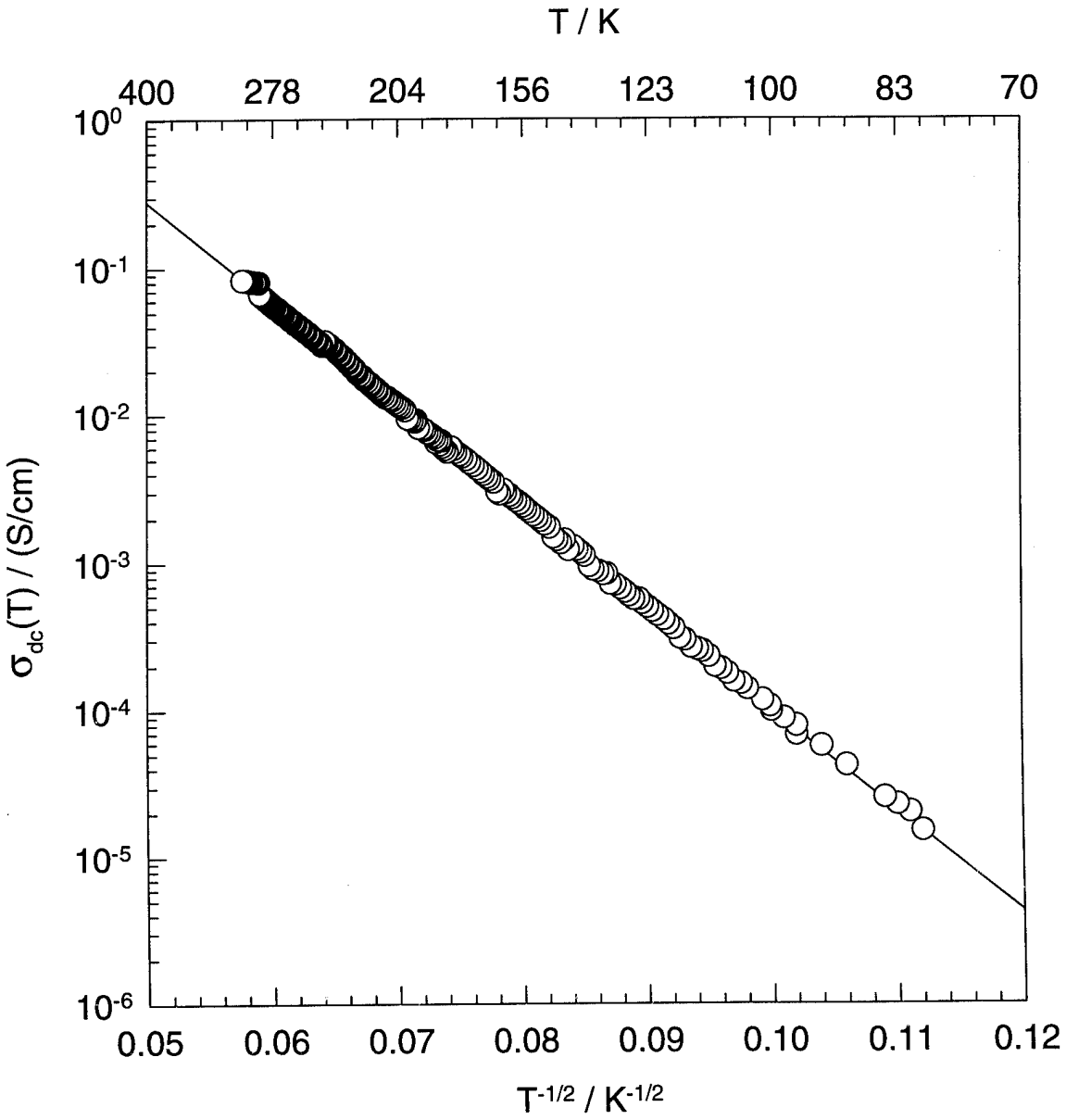

Fig. 4, Wei *et al*

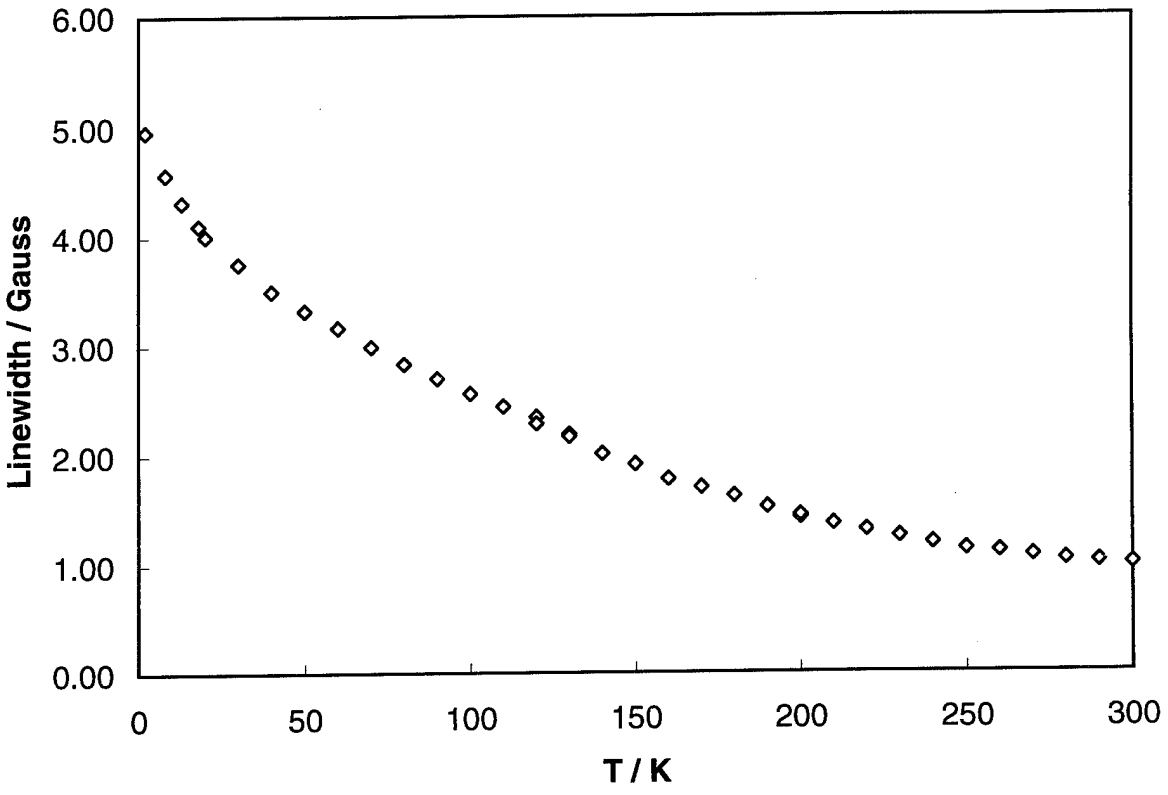

Fig. 5, Wei *et al*

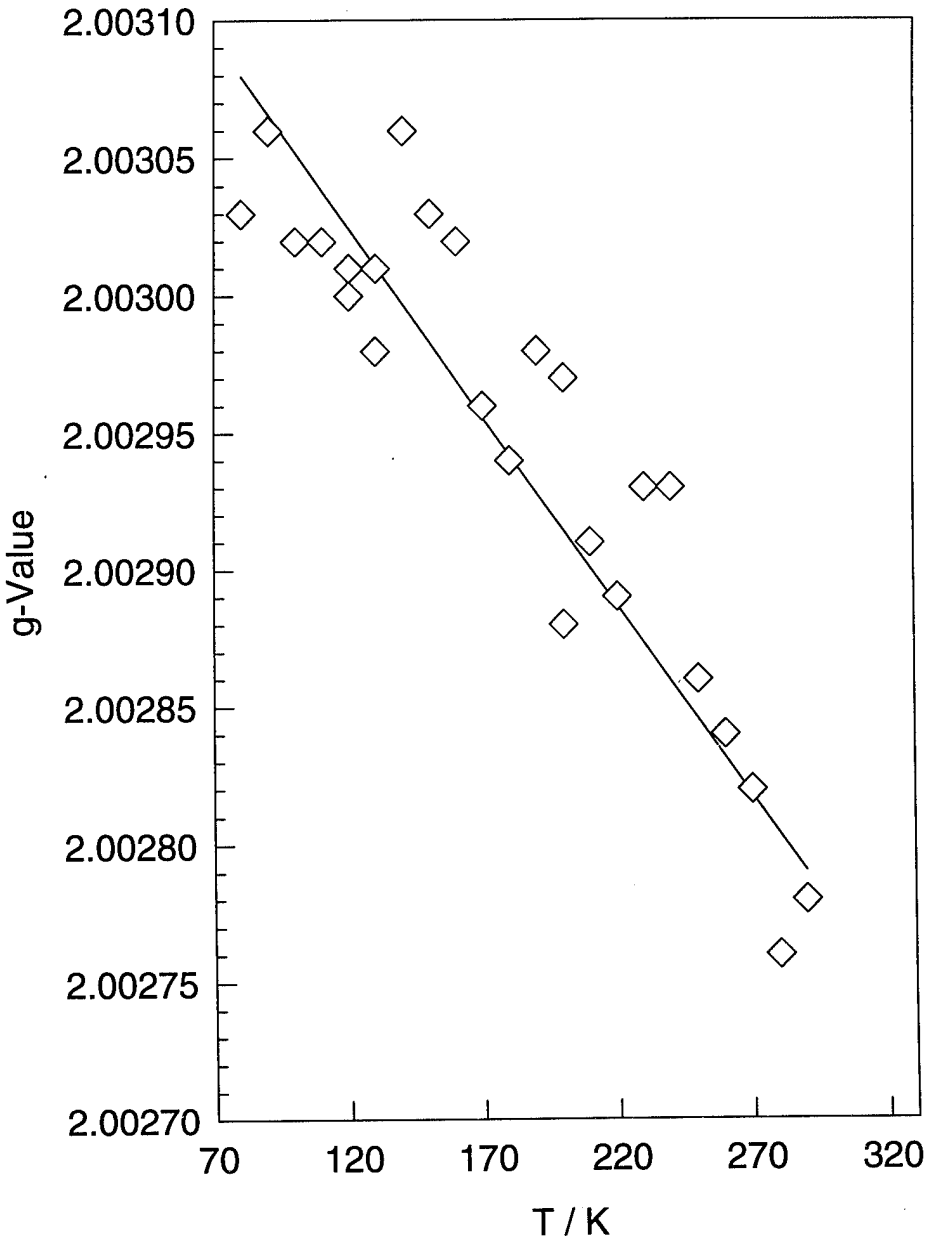

Fig. 6, Wei et al

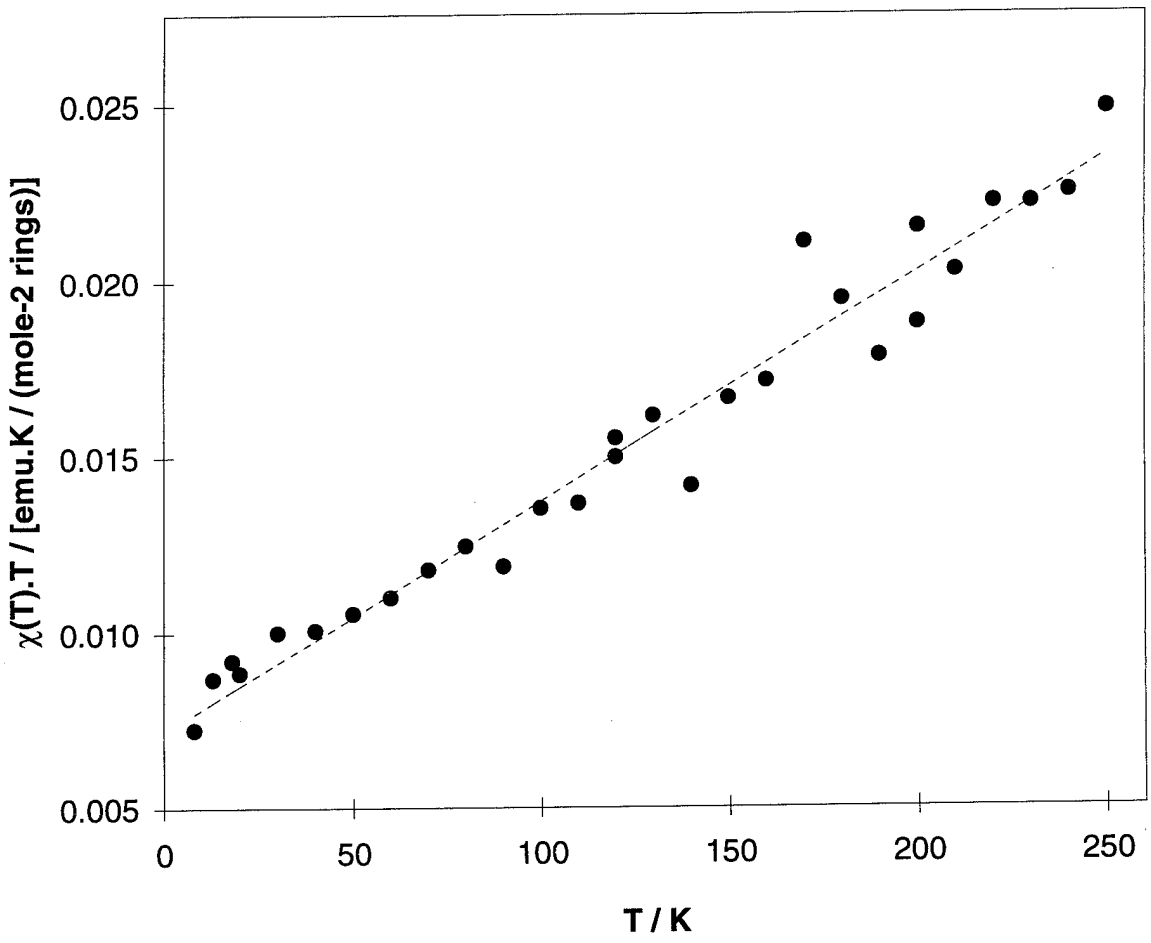

Fig. 7, Wei *et al*

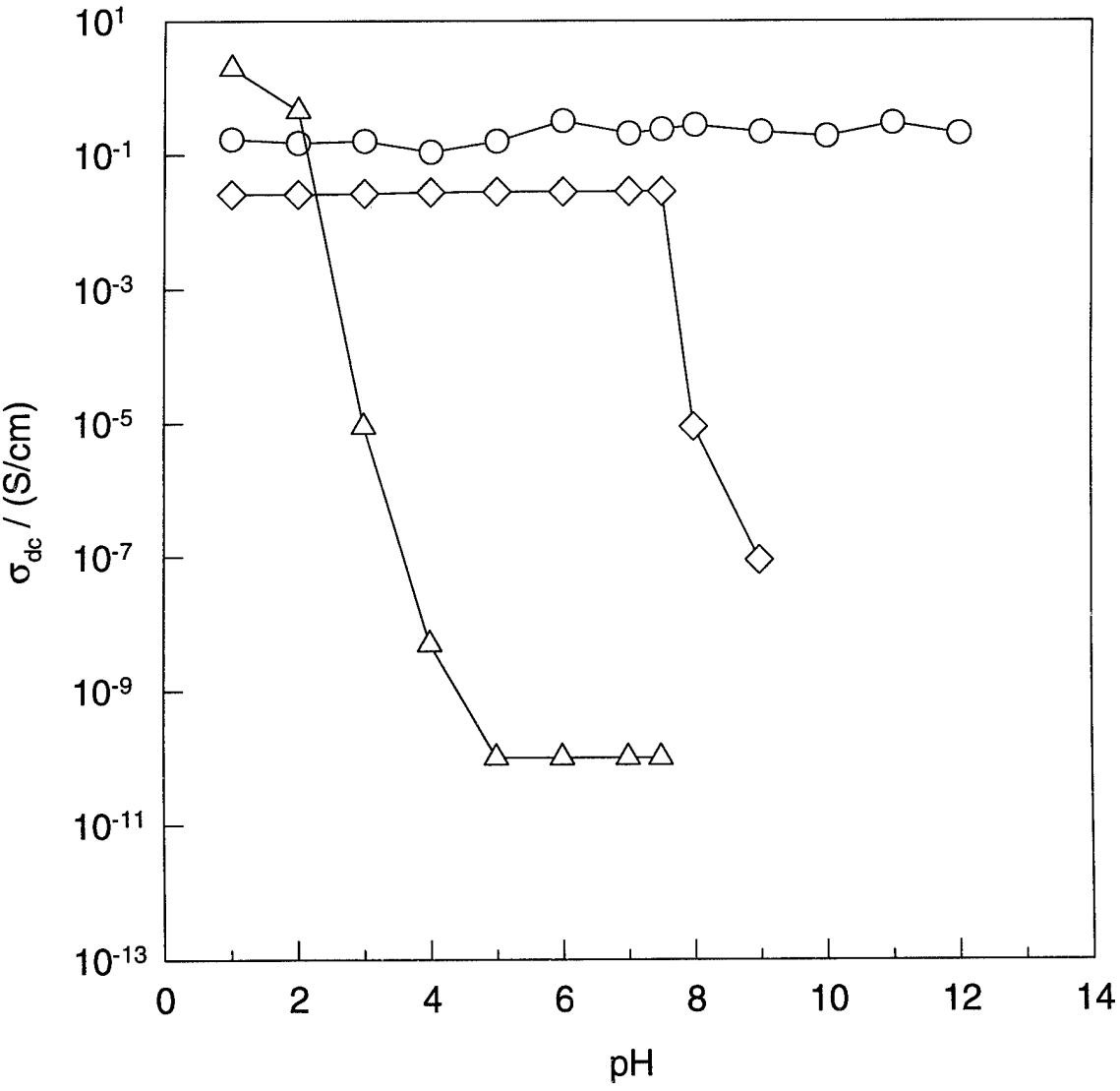

Fig. 8, Wei *et al*

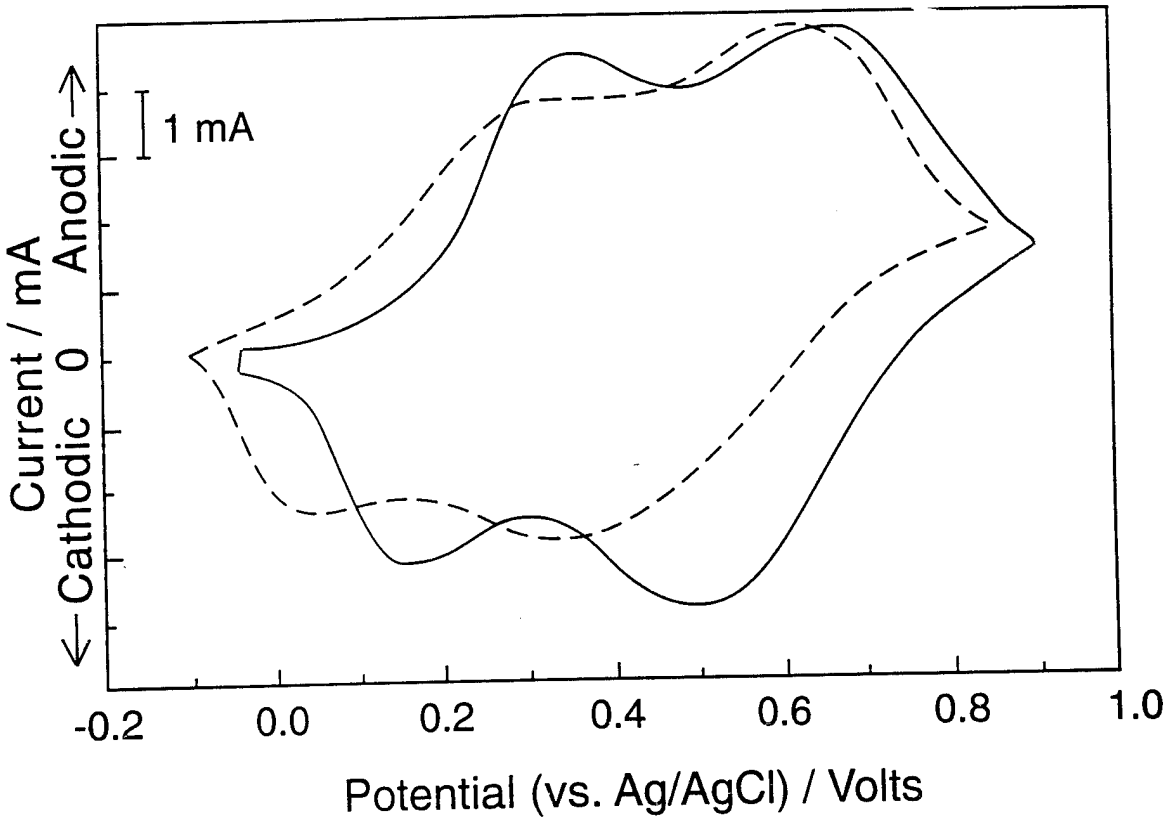

Fig. 9, Wei *et al*

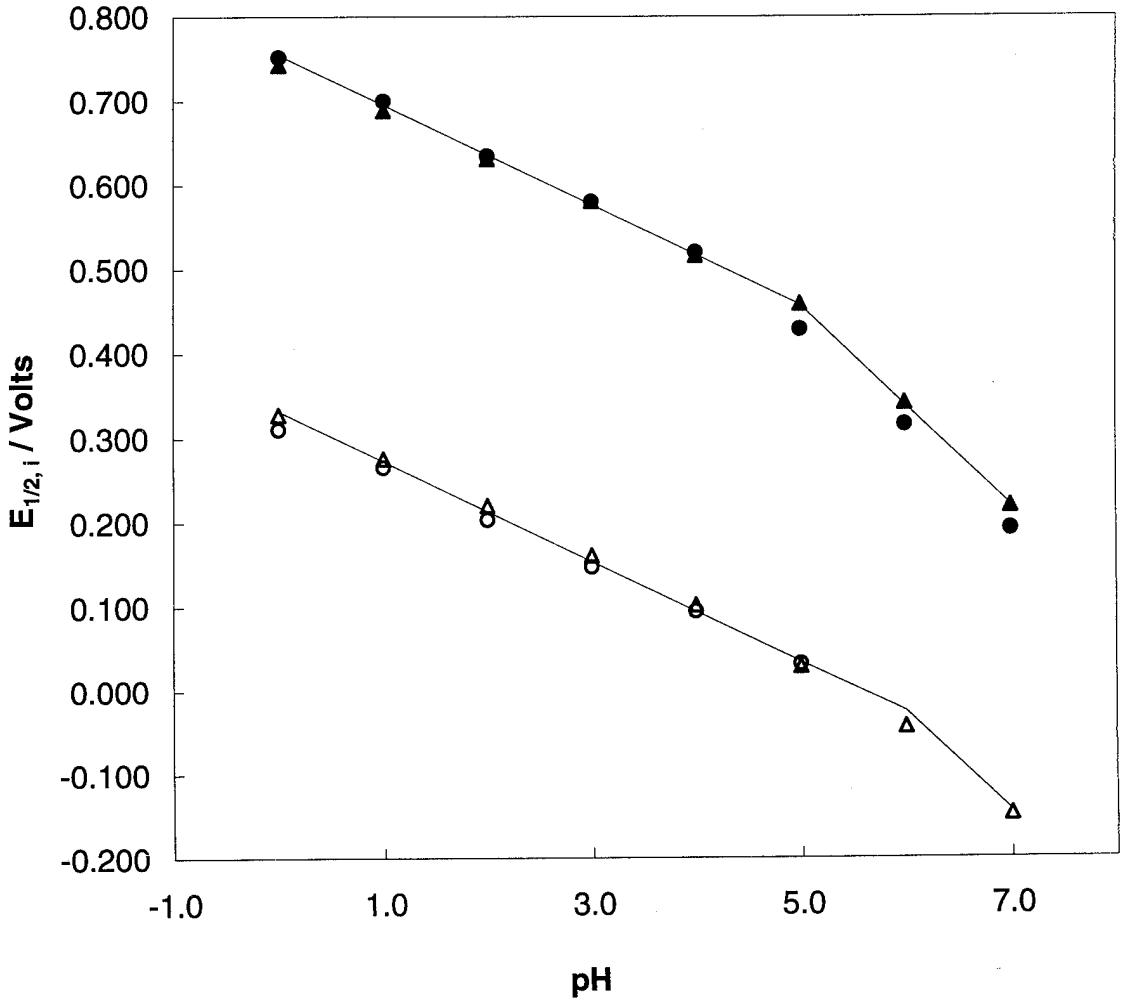

Fig. 10, Wei *et al*

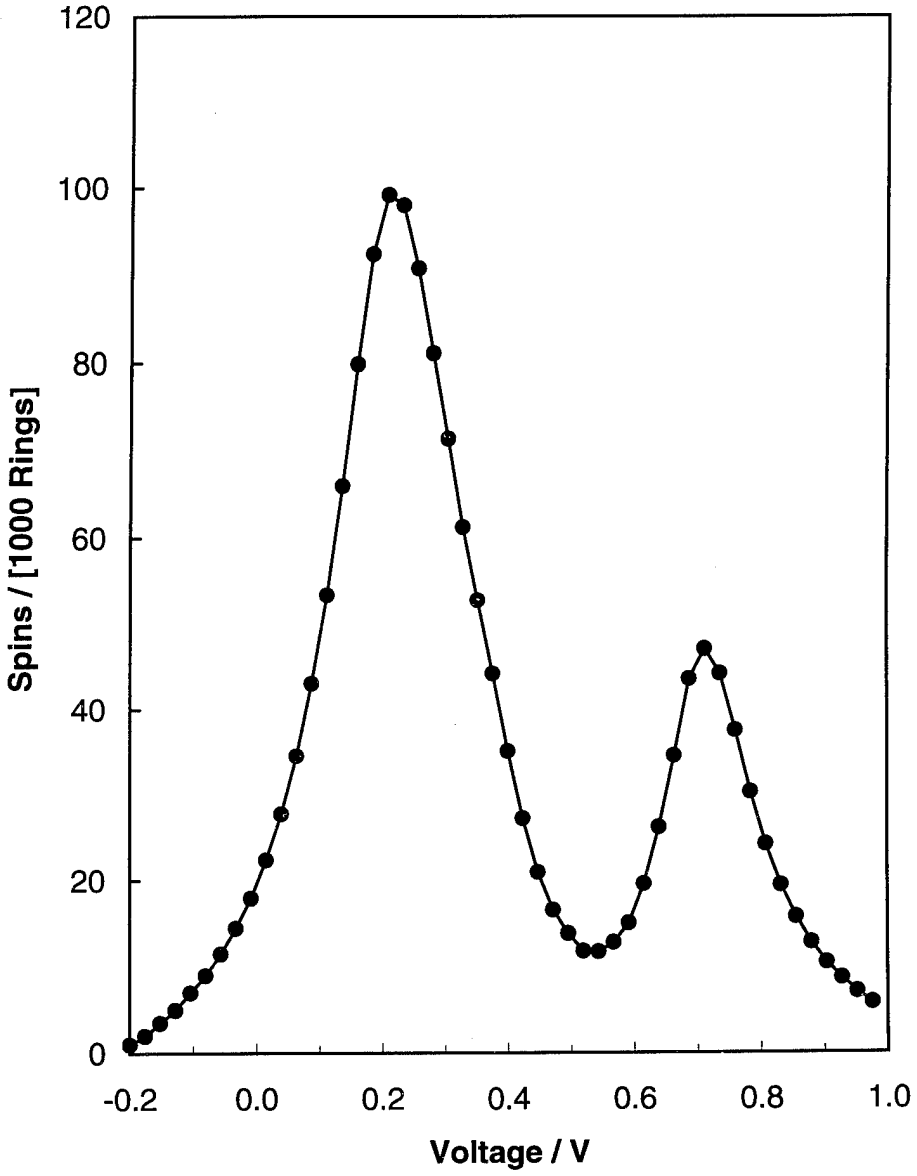

Fig. 11, Wei *et al*

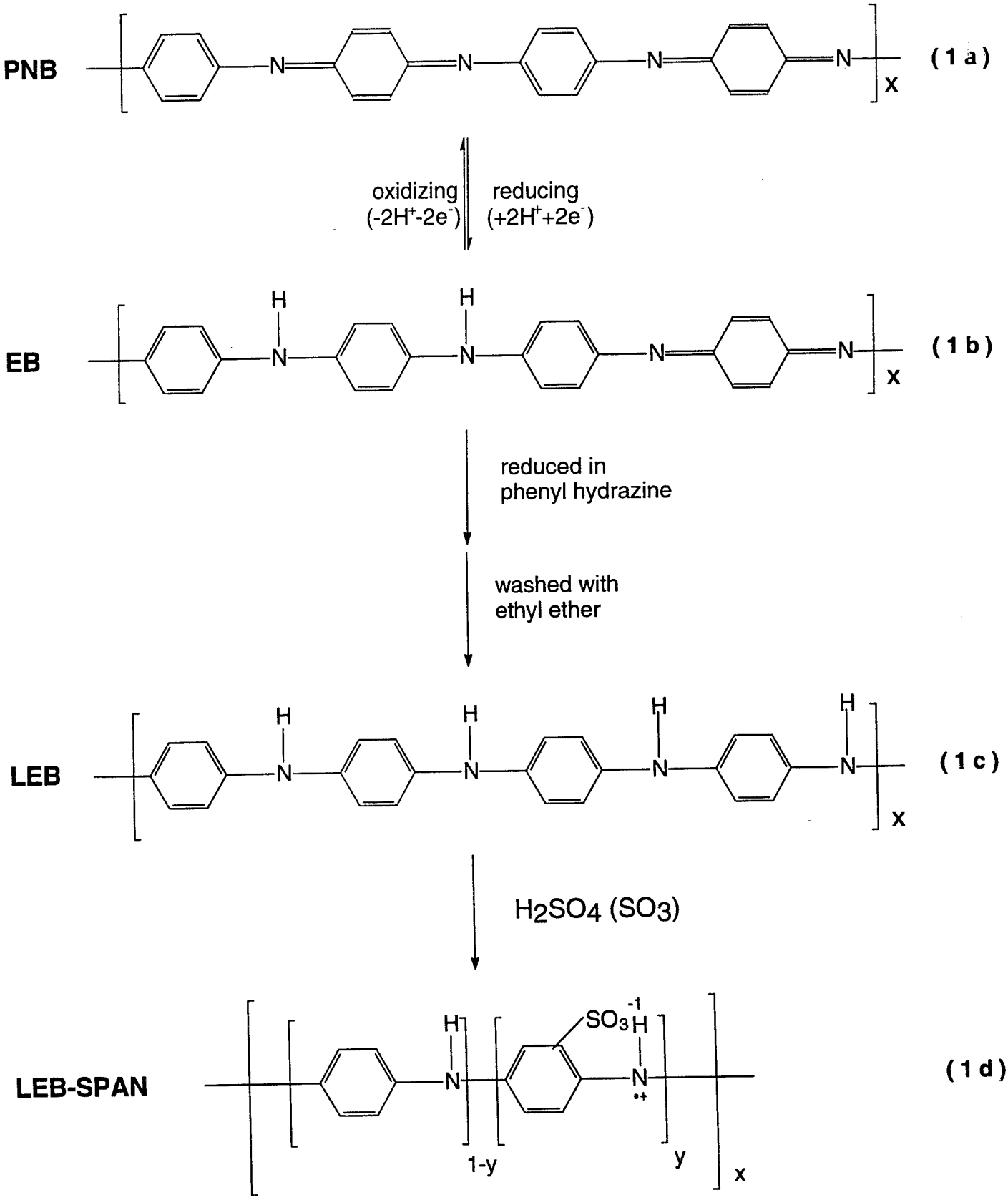
PNB
(1a)
oxidizing
(-2H+-2e-)
reducing
(+2H++2e-)
EB
(1b)
reduced in
phenyl hydrazine
washed with
ethyl ether
LEB
(1c)
H2SO4 (SO3)
LEB-SPAN
(1d)
SO3-1H
1-y
y
x

Scheme 1

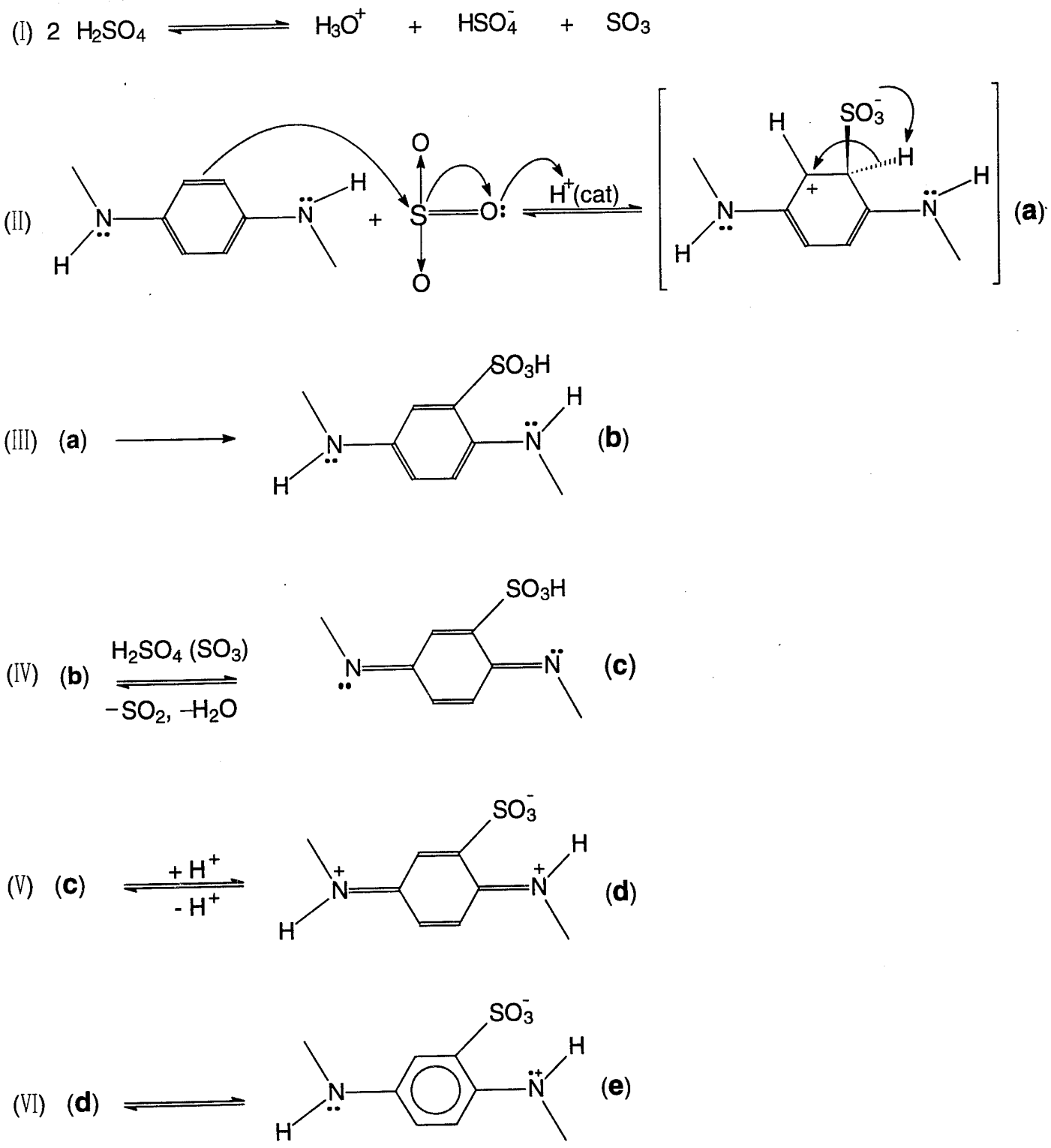
(I) 2 H2SO4 ⇌ H3O+ + HSO4- + SO3
(II)
H+(cat)
(a)
(III) (a)
(b)
(IV) (b)
H2SO4 (SO3)
−SO2, −H2O
(c)
(V) (c)
+ H+
- H+
(d)
(VI) (d)
(e)

Scheme 2

(I)

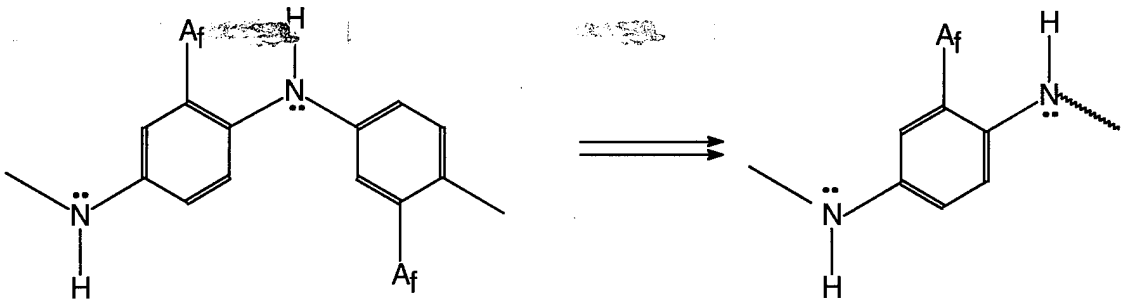

(3A) (3B)

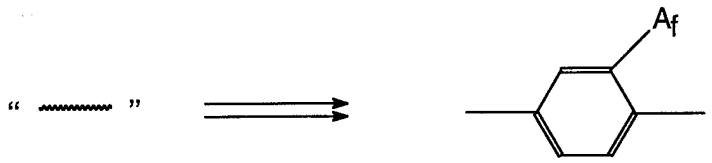

(II)

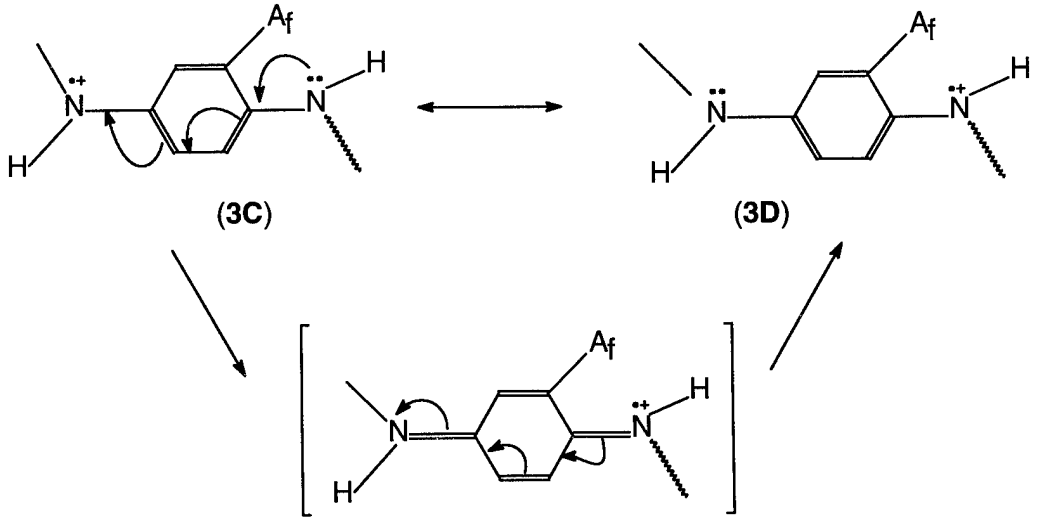

(3C) (3D)

(3CD)

Scheme 3

(I)

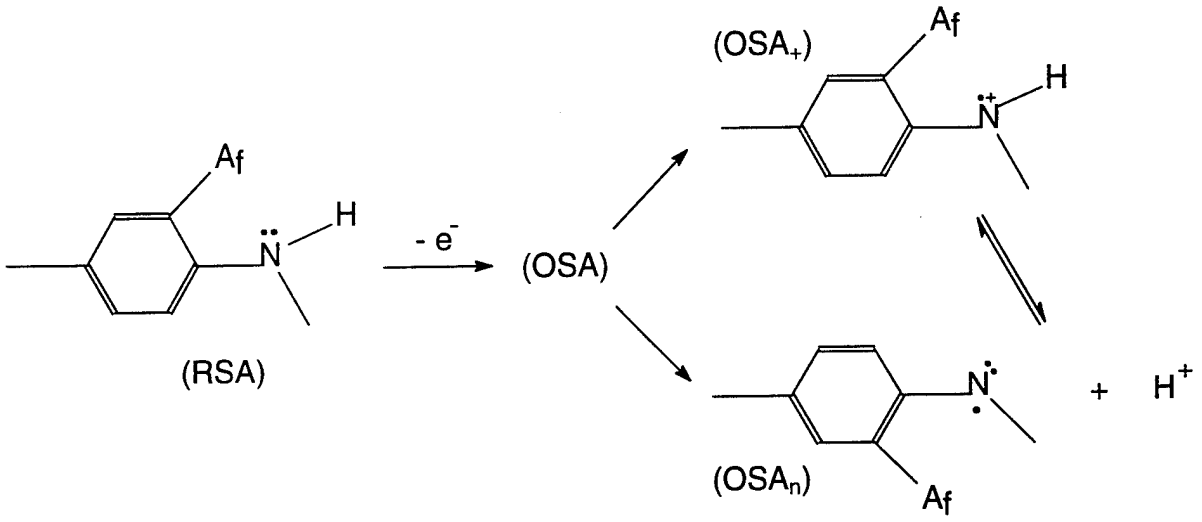

(II) Equivalently, reaction (1) can be symbolized as

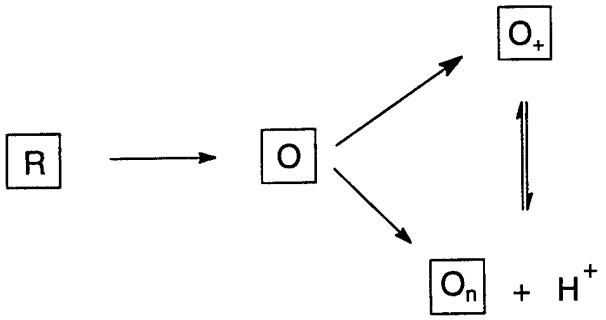

where $\boxed{R} \equiv$ (RSA);

$\boxed{O_+} \equiv (OSA_+)$;

$\boxed{O_n} \equiv (OSA_n)$;

$\boxed{O} \equiv$ (OSA), either (OSA_+) or (OSA_n).

Scheme 4

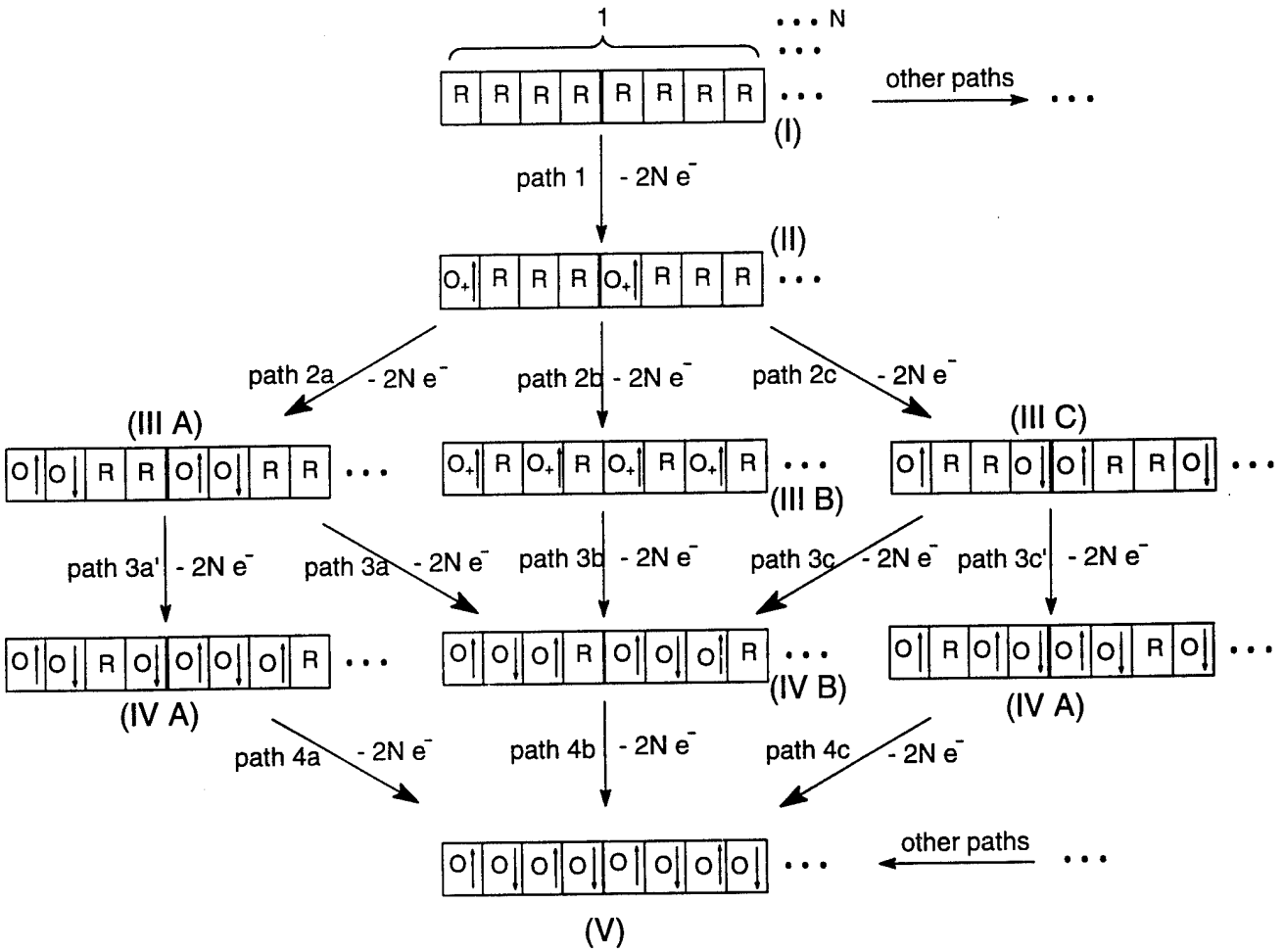

Notation:

R ≡ (RSA);

O↑ ≡ (OSA) with one spin up;

O_+↑ ≡ (OSA_+) with one spin up;

O↓ ≡ (OSA) with one spin down.

Scheme 5

(I) $$P + H^+A^- \underset{k_{deproto_1}}{\overset{k_{proto_1}}{\rightleftharpoons}} (PH)^+A^-,$$

$$(PH)^+A^- + H^+A^- \underset{k_{deproto_2}}{\overset{k_{proto_2}}{\rightleftharpoons}} (PH_2)^{2+}A^{2-}, \cdots,$$

$$(PH_{n-1})^{(n-1)+}A^{(n-1)-} + H^+A^- \underset{k_{deproto_n}}{\overset{k_{proto_n}}{\rightleftharpoons}} R^{n+} + A^{n-},$$

or simply, $$(PH_{n-1})^{(n-1)+} + H^+ \underset{k_{deproto_n}}{\overset{k_{proto_n}}{\rightleftharpoons}} (PH_n)^{n+},$$

$$K_{p,i} = \frac{k_{proto\,i}}{k_{deproto\,i}}$$

(II)

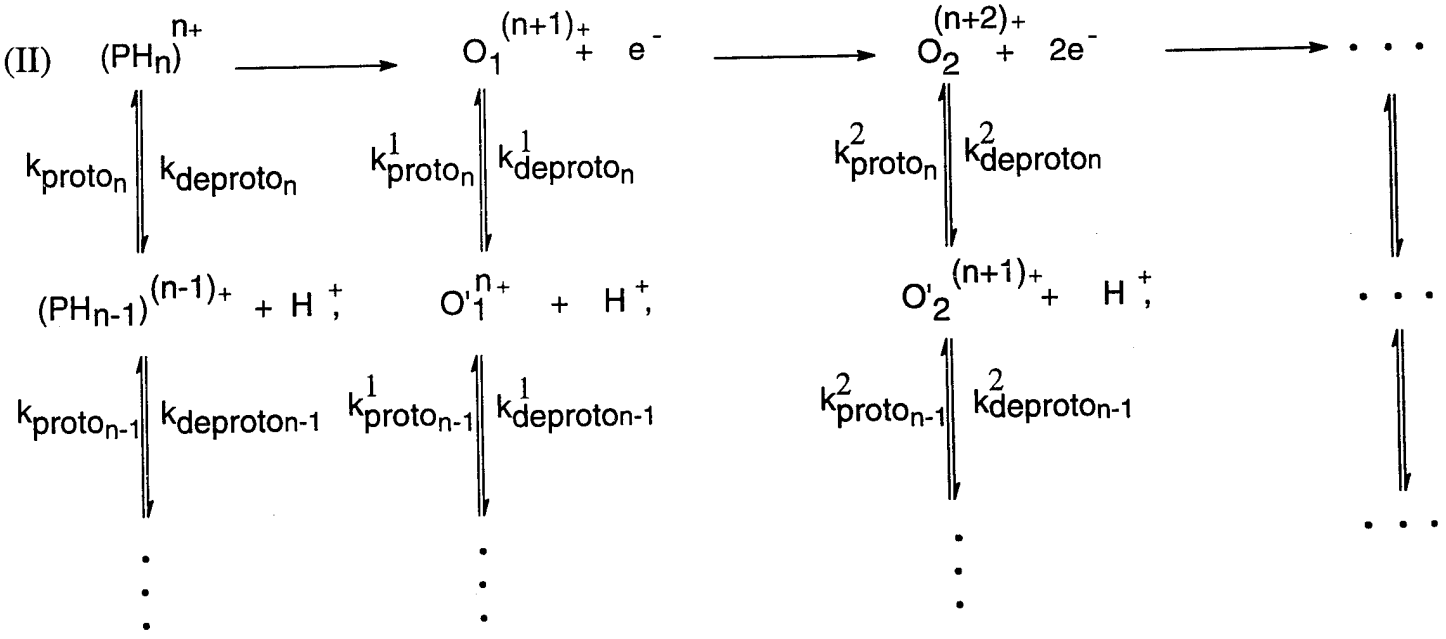

$$K^j_{d,i} = \frac{k^j_{deproto_i}}{k^j_{proto_i}} = \frac{1}{K^j_{p,i}}$$

Scheme 6

(I)

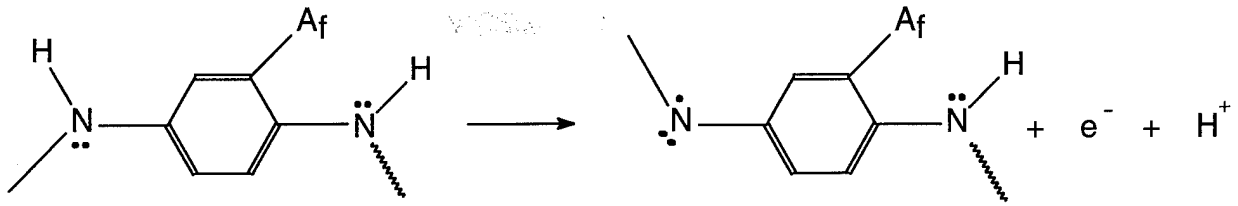

(3B) **(7E)**

(II) **(7E)**

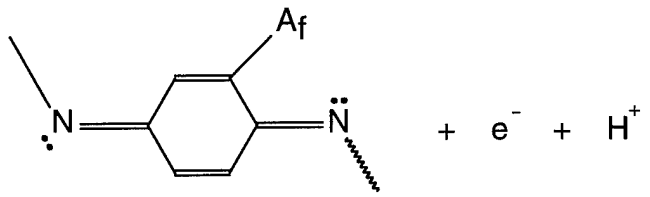

(7F)

Scheme 7

(I)

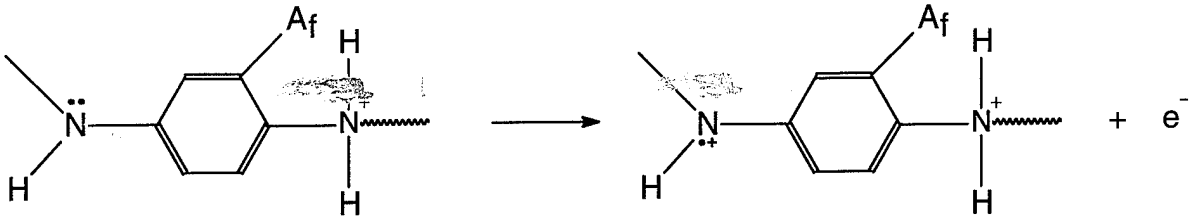

(8G) (8H)

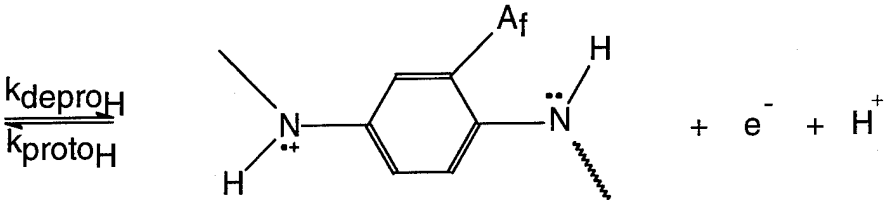

(3C)

(II) (3C)

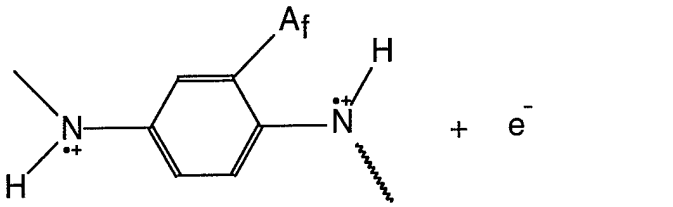

(8I)

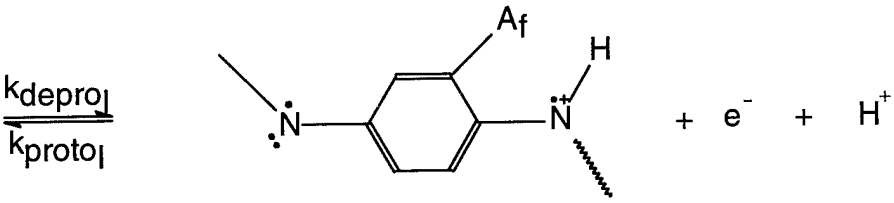

(8J)

(III) (8I)

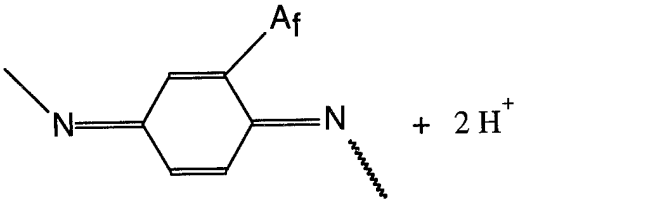

(7F)

Scheme 8

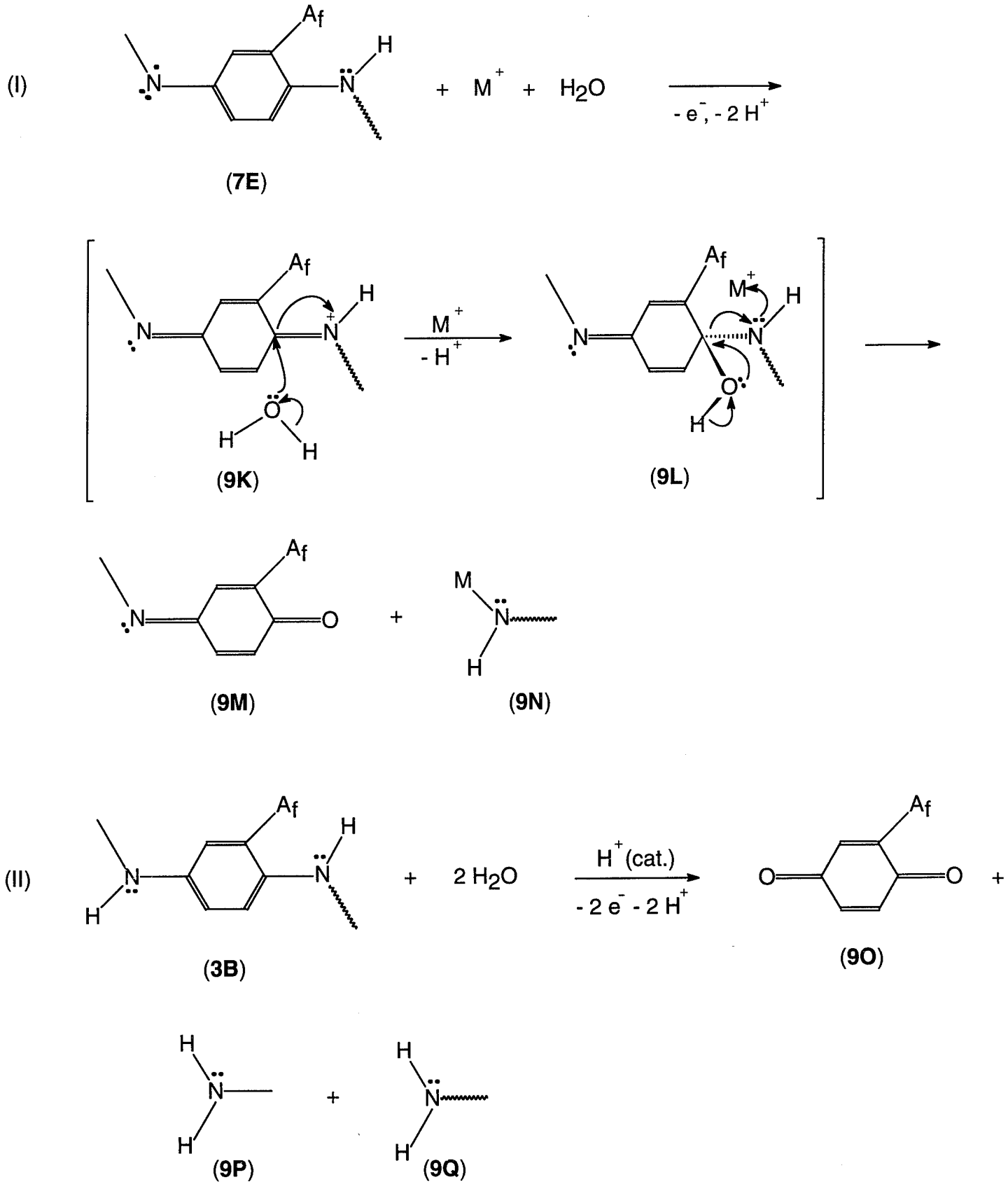
(I)
Af
H
N
N
+ M+ + H2O
- e-, - 2 H+
(7E)
M+
- H+
O
H
H
(9K)
(9L)
M
(9M)
(9N)
(II)
2 H2O
H+ (cat.)
- 2 e- - 2 H+
(3B)
(9O)
(9P)
(9Q)

Scheme 9